Physical characterization of liposomal drug formulations using multi-detector asymmetrical-flow field flow fractionation

Parot, J.[a,b], Caputo, F.[c], Mehn, D.[d], Hackley, V.A.[a], Calzolai, L.[d]

[a] Materials Measurement Science Division, National Institute of Standards and Technology, Gaithersburg, Maryland 20899-8520, United States
[b] Theiss Research, La Jolla, California 92037
[c] Université Grenoble Alpes, CEA, LETI, F-38000 Grenoble, France
[d] European Commission, Joint Research Centre (JRC), Ispra, Italy

Abstract

Liposomal formulations for the treatment of cancer and other diseases are the most common form of nanotechnology enabled pharmaceuticals (NEPs) submitted for market approval and in clinical application today. The accurate characterization of their physical-chemical properties is a key requirement; in particular, size, size distribution, shape, and physical-chemical stability are key among properties that regulators identify as critical quality attributes. Here we develop and validate an optimized method, based on multi-detector asymmetrical-flow field flow fractionation (MD-AF4) to accurately and reproducibly separate liposomal drug formulations into their component populations and to characterize their associated size and size distribution, whether monomodal or polymodal in nature. In addition, the results show that the method is suitable to measure liposomes in the presence of serum proteins and can yield information on the shape and physical stability of the structures. The optimized MD-AF4 based method has been validated across different instrument platforms, three laboratories, and multiple drug formulations following a comprehensive analysis of factors that influence the fractionation process and subsequent physical characterization. Interlaboratory reproducibility and intra-laboratory precision were evaluated, identifying sources of bias and establishing criteria for the acceptance of results. This method meets a documented high priority need in regulatory science as applied to NEPs such as Doxil and can be adapted to the measurement of other NEP forms (such as lipid nanoparticle therapeutics) with some modifications. Overall, this method will help speed up development of NEPS, and facilitate their regulatory review, ultimately leading to faster translation of innovative concepts from the bench to the clinic. Additionally, the approach used in this work (based on international collaboration between leading non-regulatory institutions) can be replicated to address other identified gaps in the analytical characterization of various classes of NEPs. Finally, a plan exists to pursue more extended interlaboratory validation studies to advance this method to a consensus international standard.

Graphical abstract

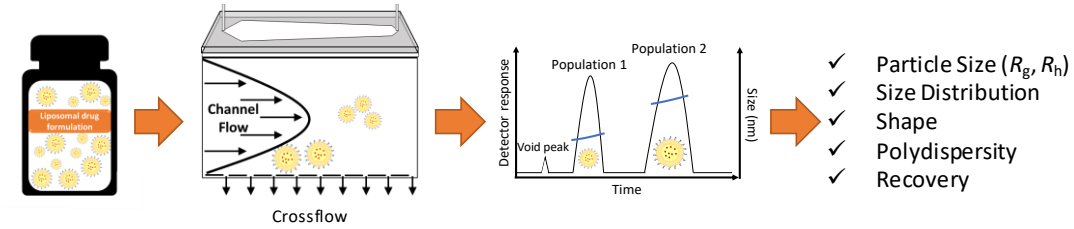

Keywords

Field Flow Fractionation, Liposome, Complex Drug, Particle Size, Physical-Chemical Characterization, Method Validation, Standardization, Regulatory

1. Introduction

Nanotechnology enabled pharmaceuticals (NEPs) are an emerging class of complex non-biological medical products offering innovative therapeutic and diagnostic opportunities [1]. In particular, liposomal formulations for the treatment of cancer and other diseases are the single most common form of NEP assessed by regulatory agencies for clinical trials and market authorization, both in the US and in the EU, followed closely by nanocrystals. The remaining 36 % include 18 different sub-classifications [2]. Despite the initial high expectations for "nanomedicine" to fundamentally alter the way disease is treated [3, 4], clinical success has been limited [5-8], in part, due to the failure to fully recognize the complex nature of NEPs and the challenges they present [9, 10]. Although progress has been slow, substantial international efforts are now underway in the nanomedicine community to accelerate the translation of promising NEPs to the clinic.

For successful translation into a clinical setting, NEPs must meet the same safety and quality criteria applied to all drug products that do not contain nanomaterials [11]. However, due to their unique and complex nature, the physical-chemical properties and biological profiles of NEPs present substantial analytical challenges relative to small molecule drugs. In general, NEPs must be evaluated using new or modified approaches that address the characteristic heterogeneous and hybrid nature of NEPs without altering the properties of interest. To further complicate matters, each NEP "subclass" is unique and may require different methodologies to evaluate similar critical quality attributes – such as size, physical structure, stability or drug loading. Clearly, a substantial gap now exists between the regulatory need to make informed decisions based on robust and validated characterization methods and the availability of such methods within the nanomedicine community [12-15]. A recent international workshop and companion article on bridging communities in nanomedicine clearly emphasized the urgent need for standardization of methods for regulatory assessment of NEPs [13]. At the moment, there are no internationally recognized standard test methods developed specifically for the physico-chemical characterization of NEPs [15]. The few nanometric standards that do exist are generic in nature (i.e., apply to "nano-objects" or "nanomaterials"), and are not generally suitable for the analysis of complex NEPs [15]. In this context, the development of more accurate and robust characterization strategies to better assess the quality and safety of different subclasses of NEPs is a key requirement for their successful translation into clinical applications. These strategies must ultimately yield robust methods that are validated across instrument platforms, laboratories and product formulations, and which identify significant sources of measurement uncertainty and artifacts.

Importantly, for physico-chemical assessment, a "one size fits all" strategy of measurement standardization has proven unreliable at best, and misleading at worst. Methods must be differentiated for different product classes, due to their unique and variable properties [13]. The US Food and Drug Administration (FDA) and the European Medicines Agency (EMA) have identified liposomal drug formulations as a *high priority* NEP class for measurement advancement and standardization focused on critical quality attributes related

to the physico-chemical state [16]. The FDA has published a guidance document for liposomal drugs that includes, among other details, a description of critical physicochemical properties [17]. Moreover, a recent summary on Standards Readiness for Nanomedicine, produced by a study group within International Organization for Standardization (ISO) Technical Committee 229 (Nanotechnologies), identified standardized methods for characterization of liposomal drug formulations as the highest priority need in the nanomedicine field. Thus, the evidence of need is clear and documented.

The present work is focused on assessment of the native physical state of NEPs, including size and size distribution – critical quality attributes relevant to all NEPs. Currently, particle size and sample polydispersity are most often assessed with dynamic light scattering (DLS) performed in batch mode. Data from FDA shows that batch DLS was used to measure particle size in 52 % of the NEP applications submitted for evaluation between 2010 and 2015, followed by laser diffraction (30 %) and then all other techniques [2]. This extensive dependence on batch mode DLS is problematic because the technique is inherently a low resolution measurement and lacks the capacity to fully resolve the size distribution of multimodal or highly polydisperse and complex samples [13, 18]. As a result, reliance on batch DLS analysis can potentially yield misleading results [12, 19-21]. Additionally, it is difficult, and often impossible, to measure the physical state and stability of NEP formulations in complex biological media using batch mode DLS. Finally, some of the other common "go-to" methods (e.g., electron microscopy) require substantial sample preparation/modification, such as deposition onto a substrate, cryogenic treatment and/or contrast staining. NEPs such as liposomes are subject to unintended alteration due to the nature of their "soft" structure, and this requires careful selection and application of measurement methodology to avoid changing the analyte as a result of the measurement or sample preparation process.

Asymmetrical-flow field flow fractionation (AF4) combined with multiple on-line detectors is a highly effective strategy to overcome the limitations of traditional batch mode DLS, while minimizing sample preparation artifacts. This hyphenated approach increases resolution of size measurements, enables analysis of complex multimodal samples and is generally compatible with complex media [22]. Multi-detector (MD) AF4 was therefore chosen for the present study due to its flexibility and broad application to biomacromolecules [23] and biomedical nanomaterials [24, 25], including lipid based systems, such as liposomes [26-33], lipid nanoparticles [20] and extracellular vesicles [34, 35], among others. In particular, MD-AF4 has the capacity to yield a rich physical dataset on NEPs, as schematically illustrated in Figure 1.

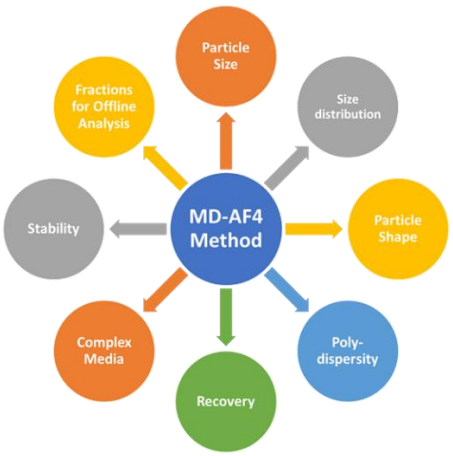

Figure 1: *The MD-AF4 method can help both drug developers and regulators alike to better characterize the physical properties of liposomal drug formulations. The method offers much more than simply size analysis, as highlighted in this diagram.*

Commercially available AF4 systems can be coupled with a wide range of on-line detectors to provide tandem measurement of size, molar mass, mass concentration, shape factor and, for many elements, composition. Fractionation occurs in the mobile liquid phase as it flows through a thin channel in which analyte diffusion is counterbalanced by a downward force provided by cross flow through an underlying porous membrane (referred to as the accumulation wall). This process results in differential particle velocities across the channel based primarily on analyte size, where smaller particles exit the channel before larger ones, and particle populations form separate bands that are detected and quantified, as represented in Figure 2. Because the particles are separated according to size, individual fractions or slices in time are essentially monodisperse, mitigating the deconvolution issue associated with batch mode DLS (and other ensemble scattering techniques).

The principal challenge for MD-AF4 is the need to develop and validate individualized methods for different NEP subclasses and, in some cases, specific formulations or even specific applications. The current work builds upon an existing ISO Technical Specification that defines the general application of AF4 to the analysis of nano-objects (ISO/TS 21362). The objective was to establish a validated best practice method based on MD-AF4 for the physical analysis (e.g., size and size distribution, modality, shape, etc.) of nanometric liposomal drug formulations.

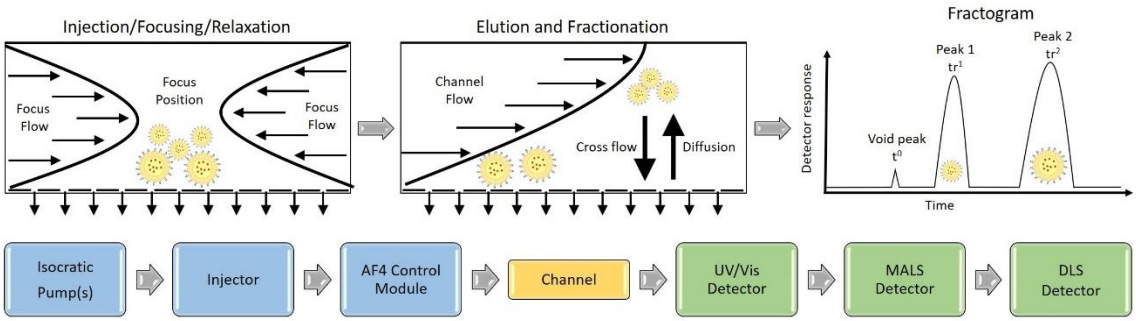

Figure 2: Top from left to right, schematic illustration of injection/focusing/relaxation step, elution with fractionation, and resulting fractogram for AF4. Bottom left to right, simplified flow diagram showing principal components of MD-AF4 instrument systems used in this study.

The prototype selected to develop and optimize the MD-AF4 analytical methodology for liposomal drugs is a research grade, monomodal, doxorubicin HCl liposome and its (drug-free) control (herein designated as Dox1 and Dox1C) [36]. The prototype possesses physico-chemical properties identical to that of the reference listed drug Doxil® (distributed as Caelyx® in the EU) [37].[1] This reference listed drug was approved by the FDA in 1995 and EMA in 1996, and has been used to treat over 600,000 cancer patients world-wide as of 2016 [38]. The formulation consists of the chemotherapy drug doxorubicin HCl crystallized within the internal aqueous cavity with ammonium sulfate in a spherical unilamellar lipid bilayer structure composed of hydrogenated soybean phosphatidylcholine, cholesterol and methoxy-polyethylene glycol (2000)-1,2-distearoyl-sn-glycero-3-phosphoethanolamine (PEG2000-DSPE). The last component is integrated with the external lipid layer providing steric stabilization and prolonged circulation by evasion of the macrophage system. The liposomes are suspended in an aqueous solution containing histidine buffer and sucrose to maintain isotonicity.

A systematic investigation was conducted with Dox1 to assess potential factors impacting the quality and reproducibility of liposome fractionation and the determination of liposome size and physical state. Based on these extensive measurements, a basic method was established and validated across different instrument platforms, laboratories and formulations. This method was then challenged using a research-grade polydisperse liposomal doxorubicin HCl product (Dox2), presenting a more complex physical state relative to Dox1. The method was further validated using two FDA-approved Doxil generics identified herein as Dox3 and Dox4. Measurement parameters were sufficiently flexible to accommodate both monodisperse and polydisperse test samples, while yielding optimal analytical parameters such as selectivity, recovery and reproducibility. The method was then successfully applied to a research-grade PEGylated liposomal ciprofloxacin (an antibiotic drug), denoted here as Cipro. Finally, the study demonstrates that the method is suitable to measure the physical properties of liposomes in complex protein-containing biological media such as plasma.

The study also identifies sources of bias and poor performance, and criteria for acceptance of data were established. We briefly address issues related to the accuracy and reliability of particle size measurements based on multi-angle light scattering (MALS) and DLS in flow mode on different instrument platforms; this topic will be more fully explored in a

[1] The identification of any commercial product or trade name does not imply endorsement or recommendation by the National Institute of Standards and Technology

subsequent publication. Critical points and good practices are identified to aid the implementation of the method.

Finally, the optimized method developed and validated in this study provides a structured yet flexible approach that can be employed across current commercial instrument platforms and applied to most if not all nanometric liposomal drug formulations. The method should be appropriate for purposes of pre-clinical research/development, product quality control and regulatory assessment. The intent is that this method will form the basis for development of an international consensus standard that expedites the regulatory review process and supports the development and broad adoption of NEPs in the treatment and detection of disease.

2. Experimental

2.1 Materials

Polystyrene (PSL) 3000 series nanosphere NIST Traceable® size standards, with nominal diameters of (30, 60, 125, 200 and 350) nm, were purchased from ThermoFisher Scientific (Waltham, MA USA). Bovine serum albumin (BSA) monomer (> 99 %), blue dextran salt and fetal bovine serum (FBS) were purchased from Sigma Aldrich (St. Louis, MO USA).

Phosphate buffered saline (PBS) used as a mobile phase in the experiments was purchased from ThermoFisher Scientific (catalog #18912), GE Healthcare Life Sciences (Pittsburgh, PA USA, catalog # 16777-252) and Lonza (Basel Switzerland, PBS catalog #17-516Q and DPBS catalog #17-512Q). Sodium chloride was purchased from Sigma Aldrich. Table S1 describes in detail the chemical composition of the mobile phase used in different experiments. Prior to measurement, the mobile phase was filtered through 0.1 µm Pall Acrodisc Supor Membrane filters obtained from VWR Scientific (Philadelphia, PA USA). Regenerated cellulose (RC) and polyethersulfone (PES) channel membranes and other channel components were purchased from Wyatt Technology (Santa Barbara, CA, USA) and Postnova Analytics GmbH (Landsberg am Lech, Germany).

The properties of the liposomal samples used in this study and the coding used to identify them in the text are summarized in Table S2. The Dox1 formulation (batch #101071) and its drug-free control Dox1C (batch #500010) were purchased from Lipocure Ltd (Jerusalem, Israel). Dox1 is sold under the name DoxoCure and its physical-chemical parameters are identical to the reference listed drug Doxil® [37]. The Dox2 sample (product code 300115, lot #300115-01-010) and its control Dox2C (product code 300116, lot #300116-01-010) were purchased from Avanti Polar Lipids (Alabaster, AL USA), and are stored frozen in 10 % sucrose and 10 mmol/L histidine buffer. Dox2 is sold under the product name DOX-NP®, but should not be confused with the previous product sold under the same tradename but manufactured by Lipocure Ltd until 2017. FDA-approved Doxil® generics were obtained through a research pharmacy. Dox3 (NDC 43598-283-35) is distributed by Dr. Reddy's Laboratories Inc. (Princeton, NJ USA) and Dox4 (NDC 47335-

050-40) is distributed by Sun Pharmaceutical Industries Inc. (Cranbury, NJ USA). Research grade PEGylated hydrogenated soybean phosphatidylcholine liposomal ciprofloxacin (product code PHPC002CP), denoted here as Cipro, was obtained from ProFoldin (Hudson, MA USA).

2.2 Sample preparation

Prior to measurement, each sample (stock suspension) was diluted into the mobile phase at a lipid concentration of 1 mg/mL and stored refrigerated at (2-4) °C until needed. Dox2 was aliquoted and stored frozen at -20 ºC (according to manufacturer directions); aliquots were allowed to thaw before use and stored refrigerated after dilution. To study the suitability of the method to analyze liposomal drugs in complex biological media, samples of Dox1 and Dox2 were diluted in PBS + 10 % volume fraction fetal bovine serum (FBS) immediately before injection. No further sample preparation was required for MD-AF4 analysis.

Best Practice Note – To maintain sample integrity, stock suspensions should be refrigerated until diluted for MD-AF4 analysis. Where high throughput analysis is required, a thermostatted autosampler is recommended.

2.3 Batch DLS measurements

Batch mode DLS measurements were performed at 25 °C using a Zetasizer Nano ZS (Malvern Panalytical, Westborough, MA USA) equipped with a 633 nm laser and operating in backscatter detection. Prior to measurements all samples were diluted in PBS at 1 mg/mL (total lipid concentration). Size results were obtained by averaging 5 consecutive measurements. The results of cumulants analysis, the mean hydrodynamic size (*Z-avg*) and polydispersity index (*PI*), are reported. Intensity-weighted hydrodynamic size distributions generated by non-negative constrained least squares (NNLS) analysis are also reported where appropriate.

2.4 MD-AF4 measurements

2.4.1 Instrumentation

Three widely available commercial platforms were utilized for this study. Included were an Eclipse DualTec (Wyatt Technology), an Eclipse AF4 (Wyatt Technology) and an AF2000 Multiflow FFF (Postnova Analytics). All platforms included necessary isocratic pump(s), degasser, injector, and fractionation channels. Additionally, each system was equipped with a minimum of three online detectors relevant to the present work: MALS, UV-Vis absorbance and DLS. For the AF2000, the DLS detector was a Zetasizer Nano ZS (Malvern Panalytical) operating in flow-mode, while for the Wyatt systems the DLS detector was integrated into the MALS. The specifications for each detector vary somewhat (e.g., angular range, number of angles for MALS), but for the purpose of the present work, all detectors were capable of performing the necessary measurements for optimization and application of methodology. For a detailed description of each system, including detectors,

refer to Supplemental Information (SI) Section 1. MALS angles for each system are shown in Table S3.

2.4.2 Fractionation

Fractograms were obtained by injecting an appropriate volume of sample into the AF4 system (typically of order 25 µL). The mobile phase (eluent) is pumped into the channel from opposite ends during injection and focusing, and exits through a replaceable semi-porous membrane at the accumulation wall (Fig. 2). When focusing is complete the analyte forms a thin line transverse to the direction of channel (and detector) flow. Subsequently the elution program is initiated, and the analyte is separated into components based on size as a result of opposing forces of particle diffusion and an applied cross flow rate (XF) perpendicular to channel or detector flow rate (DF)[2] (Fig. 2). The void peak elutes first, followed by analyte components in order of increasing size. The eluting analyte components move toward the exit port of the channel and then on to the tandem detectors. Injection, focusing, XF, DF, elution program, injected mass, membrane type and molecular weight cut-off (MWCO), mobile phase composition, channel height and length and conditioning/washing steps are optimized during method development.

The basic fractogram consists of elution time on the abscissa and detector response(s) on the ordinate axis (Fig. 2). Here t = 0 is the initiation of analyte elution with cross flow, following sample injection and focusing steps. The void time, t^0, is identified from the eluting void peak shown in Figure 2, which contains any unretained material and travels at the mean velocity of the DF. From the fractogram, analyte peaks or fractions are identified by their retention time, t_R, which is generally assigned at the peak maximum, and their retention ratio, $R=t_0/t_R$, which normalizes results to the void peak. The UV-Vis trace (mass detector) was used to define retention and void times. Unless stated otherwise, all flow rates, including injection, focus, channel/detector and cross, are given in units of mL/min (e.g., a channel flow of 0.5 mL/min is shown as DF=0.5).

2.4.3 Separation efficiency, selectivity and quality

The efficiency of a separation was assessed as a balance between the speed of analysis and the resulting resolution, while allowing multiple populations possessing different physical properties (i.e., size and shape) to be resolved if present. If relevant size standards were available, one could also assess selectivity (change in size relative to a change in retention time), but currently there are no available size standards that are suitable for the present application (i.e., for liposomes in PBS). We assessed the general quality of the fractionation by considering the shape and efficiency of the eluting peak(s), and the retention ratio (where lower values indicate increased separation from the void peak).

[2] Typically, channel and detector flow are identical, but, in some configurations, it is possible for detector flow to differ from channel flow, for instance when a post-channel or within channel splitter is used. In this study they are interchangeable terms.

2.4.4 Online size measurement

The online MALS detectors were calibrated at a scattering angle of 90° and the remaining detector angles normalized to the response at 90° using an isotropic scatterer (e.g., BSA in PBS) according to manufacturer recommendations. This process yields absolute scattering intensity (Rayleigh ratio, cm^{-1}) and ensures that all detector angles perform equally. The excess Rayleigh ratio is determined for fractionated samples (i.e., scattering from the pure mobile phase is subtracted from the sample signal). The resulting absolute intensity at 90° is typically presented in a self-normalized manner. For each "slice" or data point in a fractogram, the excess Rayleigh ratio is analyzed versus scattering angle and fit with an appropriate scattering equation (e.g., Berry form of the Debye model in the case of liposomes or the sphere form factor in the case of PSL) [39, 40]. The number of angles and angular range varies for different detectors. Data points are selected based on the quality of the fit, and the output is the root mean square radius (commonly referred to as the radius of gyration), R_g, where $R_g = \sqrt{3/5}\, R_s$ and R_s is the geometric radius of a solid sphere.

Best Practice Note: Calibration and normalization should be performed at least once per year and anytime the MALS flow cell has been disassembled (e.g., for cleaning). Normalization of all detectors to 90° should be confirmed, and, if necessary, corrected each time the mobile phase composition is changed.

Online DLS measurements were performed using either a Wyatt QELS (Quasi-Elastic Light Scattering) integrated directly with the MALS at an angle of 99.9° or 134° or using a Malvern Zetasizer positioned as the last detector and operating in flow-mode with backscatter detection at 173°. The measured correlation functions obtained during fractionation were analyzed using either single exponential decay or the cumulants method, both of which should theoretically yield the same value at the same angle if the eluting sample is size-fractionated (i.e., monodisperse). The output is the equivalent sphere hydrodynamic radius, R_h.

Where appropriate, R_g and R_h are reported on the fractogram across the full width at half maximum (FWHM) for fractionated peaks that are adequately defined, or near the peak or shoulder maximum if ill defined. In tabulated results, R_g and R_h are averaged across the FWHM (for monomodal samples) or reported at peak maxima (for polymodal samples). The spread of size values across the FWHM is reported as a measure of peak polydispersity (where spread=difference between the minimum and maximum size values across the FWHM). To perform these measurements and to present data in a fractogram format, scattering intensity at 90° is used for R_g and R_h (measured by QELS in the MALS flow cell), whereas for R_h measured using a Zetasizer in flow-mode, the detector count rate (unattenuated) at the angle of measurement (173°) is used instead. Finally, the Burchard-Stockmayer shape factor is calculated from the ratio of the root mean square radius and the hydrodynamic radius ($\rho = R_g/R_h$), where ρ=0.775 for a solid sphere and 1 for a thin hollow sphere [41].

2.4.5 Mass detection and analyte recovery

Online UV-Vis absorbance at 280 nm was utilized for mass detection during fractionation and for determination of the analyte mass recovery. Mass recovery, *R%*, was estimated by integrating the area under the UV-Vis peak for each sample eluted with and without the applied XF and focusing step, as follows:

$$R\% = \left(\frac{UV\text{–}Vis\ area\ of\ fractionated\ analyte}{UV\text{–}Vis\ area\ of\ analyte\ without\ crossflow\ or\ focus}\right) * 100; \text{ Eq. (1)}$$

For AF4, recovery is considered acceptable if analyte loss is ≤ 30 % of the total injected mass [42]. In the liposomal formulations tested in this study, an unfractionated but retained component elutes immediately after XF is removed. For present purposes, this material is included in the recovery determination (i.e., in the numerator of Eq. 1).

Explication – The unfractionated-retained peak contains material that is retained but not size separated, and which elutes only after cross flow ceases. This peak might contain, for instance, a mixture of co-eluting large structures.

Critical Point – Recovery calculations should include the unfractionated-retained peak, since technically it is not "lost" during the analytical process and is a component of the original sample.

Critical Point – Depending on the absorbance properties of the active pharmaceutical ingredient, a wavelength specific to this component can be used for recovery estimation or to differentiate between free and encapsulated drug. Additionally, other mass detectors could be used depending on the specific properties of the analytes (e.g., fluorescence, refractivity).

2.4.6 AF4 performance verification

Following the instrument manufacturer's procedure, the analyte focus position was adjusted as necessary prior to measurements. A position between (10 and 15) % of the channel length is recommended.

Prior to starting a series of measurements or after replacement of the channel membrane or following any significant alteration or maintenance on the AF4 system, (50-150) µg of BSA in PBS mobile phase was injected as a quality control material to verify performance, account for detector delays and correct for band broadening. Any unusual or unexpected fractionation results observed for BSA triggered an investigation of system integrity. BSA could also contribute to membrane passivation, but this is not the primary intent of this step and we do not believe passivation is necessary in the application of this method.

The performance and acceptable upper size range for online MALS and DLS (Wyatt QELS, Malvern Zetasizer) detectors was confirmed using NIST Traceable® PSL sphere size standards from 15 nm to 175 nm (radius) with a coefficient of variation < 3 % (AF4 PSL method in SI Section 2).

2.4.7 Uncertainty and precision

Due to the complexity, modular nature and variations in commercial platforms for MD-AF4, determination of uncertainty for multiple measurands and for the fractionation process itself are difficult to establish. For online size measurement using MALS and DLS, various models and fitting procedures are available to the user, but the calculation of underlying error is not always transparent. Uncertainty for size endpoints can be estimated by using available PSL standards, though measurements in this case are not conducted under identical conditions to the analyte. This is an especially critical issue going forward, given the increasing use of AF4-based analytical methods. On the other hand, precision (repeatability of the measurement or process) is fairly straight forward in this case. In the present study, precision was evaluated for different endpoints as the standard deviation of the mean calculated from at least 3 replicate measurements (fractionations). Replicates are considered acceptable if the calculated standard deviation is < 5 % of the mean value, as recommended in ISO TS 21362 [42].

2.4.8 MD-AF4 optimization

Method optimization was performed following the general approach outlined in Gigault *et al*. [43] and using guidelines specified in ISO TS 21362 [42]. In the first step, different elution profiles were evaluated over a range of XF/DF conditions, including constant XF, linear XF decay and exponential XF decay. Using a constant XF elution program, multiple key AF4 parameters were evaluated, including (i) short versus long trapezoidal channels (ii) membrane type and MWCO, (iii) channel (spacer) height, (vi) DF and XF, (v) focus + injection/relaxation time and focus flow rate (FF), (vi) injected analyte mass and (iv) mobile phase composition as described in Table S1 (including PBS, Dulbecco's PBS (DPBS) and isotonic saline). Additionally, other procedures were tested or varied to identify optimal conditions with respect to fractionation quality, repeatability, and recovery. For instance, memory effects were assessed and addressed by incorporating a mobile phase injection and elution procedure (sans analyte) between sample runs (infra vide).

Best Practice Note – Channel pressure should be monitored during the different steps of the focusing and elution program to ensure it remains within the manufacturer's acceptable range. Substantial or unexpected changes in pressure can indicate problems with the membrane or the flow path.

For details regarding data analysis and reporting for this method, including presentation of fractograms and assignment of retention times, refer to Supplemental Information Section 2.

3. Results and Discussion

3.1 Preliminary screening by batch mode DLS

As an initial check of sample size and polydispersity following standard industry practise, batch mode DLS measurements were performed on all liposomal samples used in the

present study. Detailed results obtained from cumulants and NNLS analysis are summarized in Table S4. Dox1, Dox3 and Dox4 yielded a Z-avg radius of 40 nm and a PI < 0.06, indicative of monomodal and relatively monodisperse samples. This conclusion is also confirmed by the intensity-based particle size distribution (PSD) analysis reported in Figure 3. Dox2, on the other hand, is characterized by a PSD shifted to larger size values and a significantly higher PI (0.26), indicative of a sample with moderate to substantial polydispersity. Moreover, the size values for Dox2 obtained by the cumulants analysis (Z-avg R_h = 56 nm) and by the intensity-weighted NNLS analysis (principal peak mean radius: 73.5 nm) differ by about 30 %. This suggests the presence of multiple populations within Dox2 that batch mode DLS, due to its low resolution, is unable to resolve. Cipro yielded a Z-avg radius of 43.5 nm and a PI of 0.01 (Table S4), again indicating a monomodal and relatively monodisperse formulation.

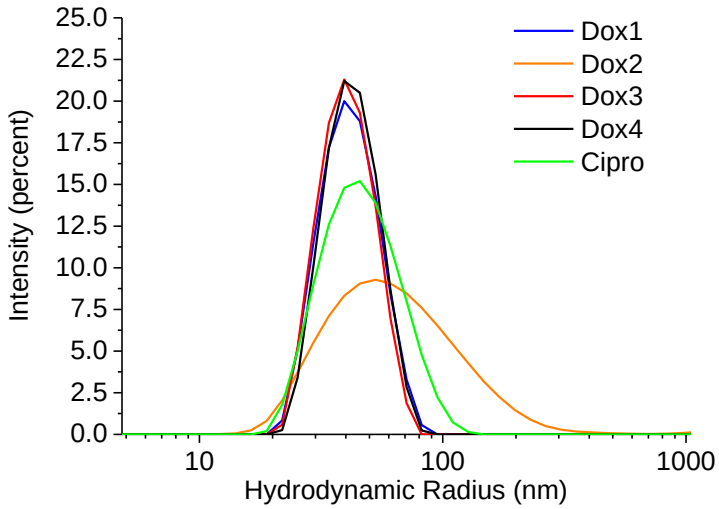

Figure 3: *Batch mode DLS: Representative intensity-weighted particle size distributions (R_h) of Dox1 (Blue), Dox2 (orange), Dox3 (red), Dox4 (black) and Cipro (green)* obtained from NNLS analysis of measured correlation data.

Batch mode DLS is not always an appropriate method to measure the mean size and PSD of NEPs, unless orthogonal data exists to support its use and interpretation. For instance, it is widely recognized that if the sample is polydisperse and/or multimodal in nature, the resolving power of batch DLS is greatly limited and can yield misleading results or limit the ability to identify significant differences between similar test samples. On the other hand, MD-AF4 offers greater capacity to resolve multiple components and to "fingerprint" the physical state of complex formulations. To obtain a more accurate PSD for these challenging materials, MD-AF4 provides substantial advantages, as discussed previously. The relevant experimental parameters were fine tuned to obtain an optimized MD-AF4 method.

Best Practice Note – Samples should be pre-screened using batch DLS to quickly provide estimates of size and polydispersity.

3.2 MD-AF4 method optimization

3.2.1 Elution program (application of cross flow)

Elution programs can be fine-tuned to improve efficiency of fractionation and speed of analysis, particularly when the sample is multimodal. Essentially, XF is varied during the elution step according to a predetermined program, where the simplest version applies a constant XF rate throughout the fractionation process. Multiple elution programs were evaluated to determine the optimal approach and to assess to what degree analysis results are impacted by the choice of program. Unless otherwise stated, the following conditions were applied during optimization of the elution program and cross flow: PBS mobile phase, long channel, 350 μm spacer, 10 kDa RC membrane, DF=0.5, FF=2 and 50 ug injected mass.

The fractograms for Dox1 are compared in Figure 4 and in Figs. S1-S2, while the mass recovery (*R*%) measured at 280 nm, t_R, *R*, the mean and spread of R_g and R_h are reported in Tables S5-S8. Mass recovery was always > 90 %, for all programs tested. However, different programs yielded different fractogram profiles, with the maximum elution time at 13.53 min for constant XF at 0.3, 19.29 min for the exponential decay from XF=1.0 to 0 in 60 min, and 23.36 min for the linear decay from XF=1.0 to 0 in 30 min.

On the other hand, the size profiles and the quality of the separation for almost all programs tested are remarkably similar for Dox1; that is, the data indicates a single population with a mean R_g of about 30 nm, a mean R_h of about 35 nm, a size spread (max-min value at the FWHM) of about 10 nm, and a Burchard-Stockmayer shape factor ($\rho = R_g/R_h$) of 0.84. The shape factor is intermediate between the theoretical value for a solid sphere (0.77) and that for a thin hollow sphere (1.0), and is therefore consistent with the known structure of doxorubicin HCl encapsulated liposomes (i.e., a core shell structure where the core is not empty, but not uniformly solid either). The difference might also be within the statistical uncertainty of this ratio determination. The only exception here was the long linear decay (45 min or longer), which resulted in broad asymmetric peaks (see SI, Fig. S1B and Fig. S1C). Even if the efficiency of separation of the analyzed monomodal sample is satisfactory for all profiles tested, the constant XF profile might have better selectivity and resolution when analyzing multimodal samples (though potentially at the expense of speed of analysis). For this reason, and also because of its simplicity in method development across different instrument platforms and software packages, the constant XF program was selected for further method optimization, with XF=0.3. The XF value was selected based on a comparison of fractionation results (data not shown) obtained for DF=0.5 and higher; this XF value generally worked well for all liposomal formulations tested.

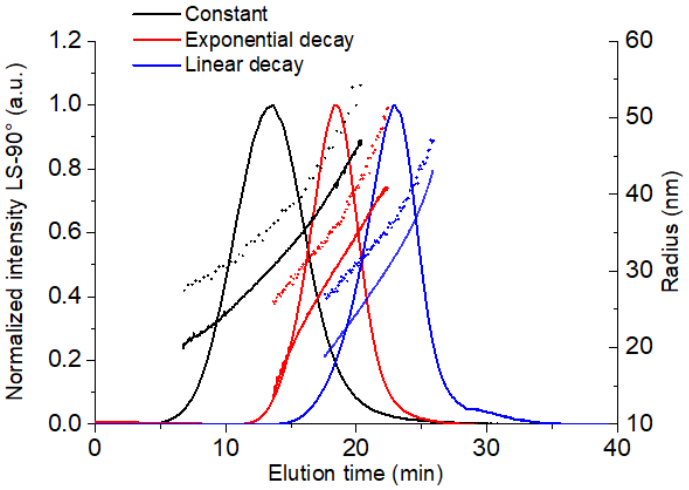

Figure 4: Comparison of elution programs applied to Dox1. AF4 fractograms resulting from different elution programs (normalized excess Rayleigh ratio at 90°), R_g (line) and the R_h (dots) as a function of elution time for injection of 25 µg of Dox1. Constant XF = 0.3 (black), exponential decay from XF=1.0 to 0 in 60 min (red) and linear decay from XF=1.0 to 0 in 30 min (blue).

3.2.2 Detector flow rate and determination of upper size limits

DF was optimized by evaluating its effect on the retention time, separation selectivity and recovery. Unless otherwise stated, the following conditions were applied during optimization of DF: PBS mobile phase, short channel, 350 µm spacer, 10 kDa RC membrane, XF=0.3, FF=2 and 25 ug injected mass. Varying DF from 0.5 to 1 did not significantly impact the separation selectivity or analyte recovery, though it does impact the peak breadth somewhat (see Fig. 6F). Importantly, its influence on the upper size limit measurable by the online DLS detectors was considered. It is known that DF can impact the upper size measurable by online DLS detectors [44], while MALS is much less sensitive. In flow mode, the slower Brownian motion (and longer correlation decay time) of larger particles requires a longer residence time in the measurement zone to be accurately analyzed by DLS. The larger the particle the longer the correlation decay. For this reason, online DLS measurements tend to underestimate the R_h values, and the systematic error in the R_h measurements is larger, when higher DF rates are applied and/or larger particles are measured.

In order to assess the suitability of the online size detectors used in typical instrumental setups in the size range relevant for most liposomal formulations (i.e., radius from about 15 nm to about 100 nm) we first measured PSL size standards of nominally (15, 30, 62.5, 75, and 100) nm radius by applying two different flow rates: DF=0.5 and 1, which covers the typical range of use for AF4. The performance of the MALS detector, the QELS detector at two angle positions (99.9° and 134°) and the Zetasizer (in flow-mode) were

analyzed. The fractograms are plotted in Figure 5, while the mean size values calculated across the FWHM are summarized in Table S9. Size calculated by MALS using the sphere form factor (i.e., the sphere model) was always consistent with the stated size value, and constant across the eluting peak (as expected for single mode monodisperse populations). In contrast, the QELS position/angle directly affects the R_h values with better accuracy at position 16 (scattering angle 134°) in comparison with position 12 (scattering angle 99.9°) for particles larger than 75 nm (radius). Using position 12, R_h values for PSL ≥ 75 nm were underestimated, while at position 16 results were acceptable up to 175 nm (Table S9). This effect is well known to the instrument manufacturer, who has developed a larger bore cell for applications involving larger particles (> 75 nm) independently of the QELS position. The manufacturer also recommends installing the QELS detector at a higher angle (e.g., position 16) in the standard MALS flow cell for larger size particles (e.g., R_h > 75 nm). Consequently, the two QELS positions (12 and 16) can be used to measure the size range relevant for most liposomal drug formulations. Therefore, we conclude that the upper size limit will be slightly reduced at DF=1 compared to 0.5. However, even at DF=0.5, in our configuration, the upper size limit for DLS using the Wyatt QELS integrated detector with the standard flow cell is about 75 nm (radius), while no upper size limit was observed for the MALS detector (R_g) within the diameter range evaluated. The vendor (Wyatt) states in their literature that the applicable R_g range for the configuration and laser wavelength used in this study is from about (10 to 250) nm. Therefore, when using the Wyatt MALS/QELS combined detector with the standard flow cell, it is recommended that the analyst rely on R_g alone for size when the measured R_h is larger than about 75 nm. For the Zetasizer DLS operating in flow-mode as the final tandem detector, no upper size limit was observed using PSLs up to 100 nm in radius, at DF=0.5 or 1. However, to obtain acceptable R_h results from the Zetasizer in flow-mode, it might be necessary to increase the injected analyte mass relative to that used with the online QELS. This depends strongly on the size and scattering properties of the analyte.

Critical Point – The angle of DLS measurement can significantly affect the measured R_h. This effect becomes more noticeable as particle size increases.

Best Practice Note – The upper size limit for R_h measurements on a given instrument platform should be confirmed using size standards over a range that is relevant for the target analyte.

Notably, for Dox1, which is below the upper R_h limits established in this study, the R_h values calculated at higher DF were nevertheless slightly smaller compared with lower DF, even though separation selectivity and recovery results were acceptable at either flow rate (see Table S10 and Fig. S3). In order to minimize potential bias induced by DF on the measured R_h values we selected DF=0.5 for further optimization, as it offered a larger operational range and consistent R_h values.

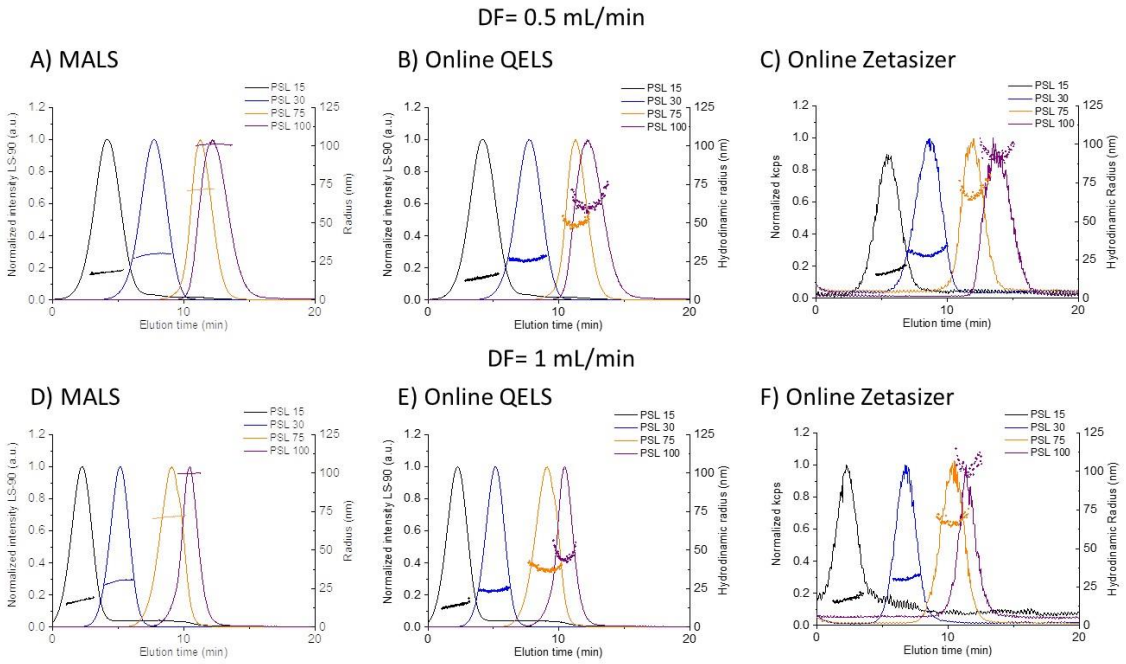

Figure 5: *Determination of the upper size limits using online detectors. AF4 fractograms (normalized excess Rayleigh ratio at 90°) for PSL (15-100) nm (radius) with R_h at FWHM (dots) overlaid. (Top) A) MALS (Wyatt), B) online QELS and C) online Zetasizer (Malvern) measured at DF=0.5. (Bottom) radius measured at DF=1.0 by D) MALS, E) online QELS and F) online Zetasizer.*

3.2.3 Channel and membrane properties

The influence of key channel parameters (i.e., channel length, spacer thickness and membrane type/MWCO) on the fractionation process was evaluated for Dox1. Unless otherwise stated, the following conditions were applied during optimization of the channel and membrane properties: PBS mobile phase, DF=0.5, FF=2, XF=0.3 and 25 ug injected mass. Channel length does not affect separation selectivity, mass recovery or the measured size values (see Fig. 6A and in Table S11). Therefore, both the standard "long" (275 mm) and "short" (145 mm) channels from Wyatt can be applied in the method with similar results. The benefit to using the shorter channel is a reduction in analysis time and potentially some reduction in band broadening (though significant band broadening was not observed with Dox1), while the long channel more closely matches the standard channel length (280 mm) used on the Postnova platform. All channels tested use the standard trapezoidal geometry (where the channel breadth decreases toward the outlet), as it regulates the channel flow velocity and minimizes band broadening [45].

Three spacers were evaluated to establish the effect of channel height, which directly impacts the parabolic velocity profile (see Fig. 2) between the accumulation wall (membrane surface) and the solid channel top called the depletion wall; *viz.* 250 µm, 350 µm and 490 µm (see Fig. 6B and Table S12). Based on these tests, the 350 µm spacer was selected as the best compromise to minimize peak broadening and retention time,

while achieving good detector sensitivity (a function of sample loading and dilution) and retention ratio (separation from the void peak).

Finally, we assessed the two most commonly used and widely available membrane materials for AF4; *viz*. RC and PES. For this comparison, membranes with 10 kDa MWCO were used for fractionation of Dox1. As summarized in Table S13 and shown in Figure 6C, the PES membrane increased analyte loss compared to RC, though the mass recovery was above 70 % (and thus acceptable) for both. In addition, the PES membrane resulted in increased retention time and peak broadening, indicating there is greater interaction between PES and the liposomes compared with RC. From this we conclude that RC is a better choice for optimization. As shown in Table S13, the two most common MWCO values were compared, 10 kDa and 30 kDa. The principal effect of MWCO is on retention time and channel pressure during elution (data not show). Otherwise, the results and separation efficiencies appear similar. Based on this data, we conclude that either MWCO value will work for separation of liposomal drugs; 10 kDa was chosen for further optimization because it is more commonly employed for separations involving nanomaterials.

3.2.4 Mobile phase

Mobile phase composition is likely the most critical variable with respect to optimizing an AF4 method. It impacts nearly every aspect of the fractionation process, and the analyst has a wide range of options to choose from in order to enhance method performance while minimizing alteration to the analyte during the fractionation process. Unless otherwise stated, the following conditions were applied during evaluation of the mobile phase: short channel, 350 µm spacer, 10 kDa RC membrane, DF=0.5, FF=2, XF=0.3 and 25 ug injected mass. For NEPs, it is important to measure their properties in a representative state, so an isotonic mobile phase at physiological pH is generally recommended. In the present study, fractionation was evaluated using unbuffered isotonic saline (pH 6) and PBS buffers (pH 7.2 to 7.4) purchased from different sources and which are characterized by slightly different chemical compositions (see Table S1 for details). The results, reported in Figure 6D and in Table S14, show that all tested mobile phase compositions yield similar or nearly identical results, based on sample recovery, separation efficiency and the measured sizes. PBS was selected here as the principal mobile phase because it provides near isotonic dilution of the liposomal formulations (avoiding potential adverse osmotic effects, such as impacting release of the active pharmaceutical ingredient), its pH is in the physiologic range and it is chemically stable. Additionally, PBS has been widely used as a dilution medium for studies of liposomal drug formulations reported in the literature.

Best Practice Note – While the composition of PBS media can vary, and pH can range from 7.2 to 7.5, PEGylated liposomes exhibit nearly identical fractionation behavior regardless of these variations. We conclude that the source of PBS is not a significant factor, at least within the range evaluated here.

3.2.5 Focus and relaxation

The focus time and FF are critical parameters for an MD-AF4 method. If focusing is not appropriately set, the separation can be directly affected, and results misinterpreted. The processes involved during injection/focus/relaxation are crucial for the subsequent elution/fractionation/detection processes. A poorly optimized focus/relaxation step can result in sample loss, a void peak with substantial entrainment of analyte and distorted or broadened peaks. The focus/relaxation step was optimized by analyzing FF and the focusing time. Unless otherwise stated, the following conditions were applied during optimization of focus and relaxation: PBS mobile phase, short channel, 350 µm spacer, 10 kDa RC membrane, DF=0.5, XF=0.3 and 25 ug injected mass.

Initially, FF was varied from 1 to 2 with no observable effect (data not shown). Then FF was fixed at 2 and focus times of (3, 5, and 8) min were tested. Surprisingly, results (Fig. 6E and Table S15-S16) show that focus time has virtually no impact on fractionation of Dox1, so a focus time of 8 min was selected for the optimized method to ensure the formation of a uniform analyte band prior to elution. However, results indicate that shorter focus times can be applied in situations where 8 min is observed to induce agglomeration in the channel and/or result in low recovery. We emphasize that these effects were not observed for the PEGylated liposomes investigated in the present study.

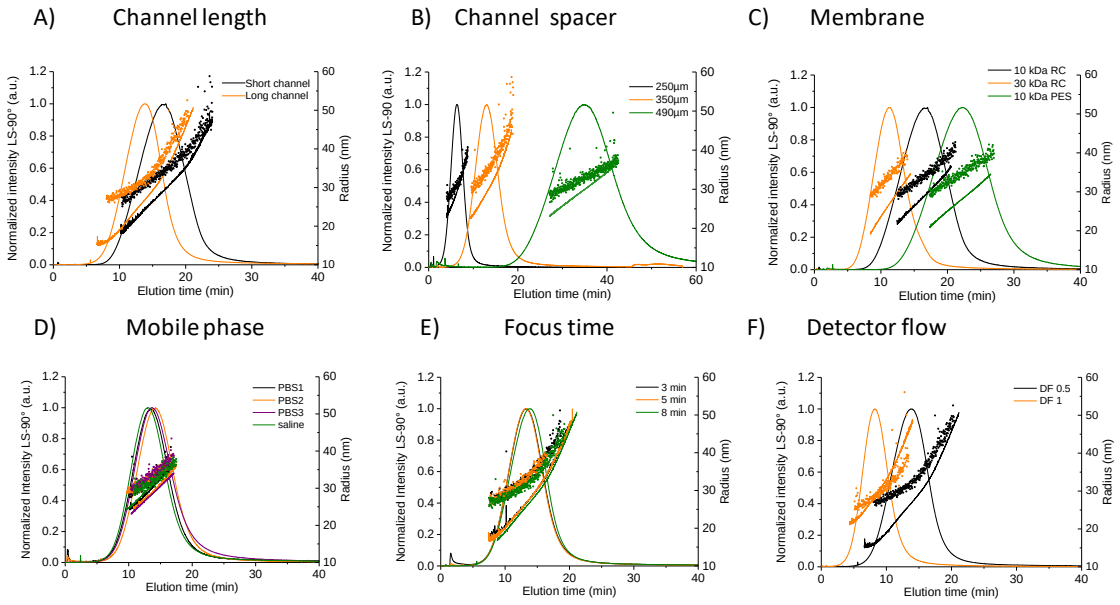

Figure 6: Method optimization results for Dox1. Fractograms showing the elution trace (normalized excess Rayleigh ratio at 90°), R_g (line) and R_h (dots) versus elution time for injection of 25 µg Dox1, constant XF=0.3 and varying A) channel length (black: short channel, orange: long channel, B) channel spacer (black: 250µm, orange: 350µm, green:490µm), C) membrane (black: RC 10 kDa, orange RC 30 kDa, green: PES 10 kDa) D) mobile phase (green: isotonic saline=NaCl 0.9%, black: PBS from Lonza (PBS1), orange: DPBS from Lonza (PBS2), purple: PBS from Hyclone (PBS3), E) focus time

(black: 3 min, orange: 5 min, green: 8 min) and F) detector flow (violet: 0.5 mL/min, green: 1.0 mL/min) are reported.

3.2.6 Sample mass

The mass of injected analyte (based on lipid content) impacts the fractionation process as well as the detector response. If the mass is too low, detector sensitivity will be compromised. If the mass is too high (referred to as overloading), detectors will saturate and fractionation can be adversely affected (e.g., coelution, where different size particles elute together instead of at different retention times or retained material that is not fractionated). The correct range will depend to some extent on the optical scattering properties and size of the analyte and is best evaluated by injecting a series of known masses under conditions appropriate for the intended analysis. The resulting fractograms can then be compared with respect to detector signal/noise and peak quality as well as analyte recovery. The objective is to identify a mass range that provides sufficient signal/noise, without saturating detectors or inducing memory effects and/or compromised recovery. Unless otherwise stated, the following conditions were applied during optimization of injected mass: PBS mobile phase, short channel, 350 µm spacer, 10 kDa RC membrane, DF=0.5, FF=2 and XF=0.3.

As shown in Figure 7(B-C), for injected mass of Dox1 < 15 µg, the noise of the scattering intensity trace registered by either MALS or QELS sensors is high, even across the peak FWHM, thereby degrading the capacity to measure reliable size values (Table S17). Alternatively, no loss of resolution or reduction in t_R due to channel overloading was observed for the conditions tested at injected mass up to 200 µg. It is notable that R_h degrades (becomes noisier) faster with decreasing mass relative to MALS derived R_g, an effect observed for other analytes as well. On the other hand, the response of the mass sensitive UV-Vis signal at 280 nm (Fig. 7A) is linear over the tested range. To minimize sample consumption, avoid potential memory effects and maintain an appropriate signal/noise for light scattering detectors, (25 to 50) µg was identified as the optimal range for injected mass of liposomal formulations.

Critical Point – Although injected mass must be controlled, the injected volume can vary since excess liquid will be removed through the membrane during injection/focusing. Therefore, if sensitivity is an issue for a low concentration sample, a larger volume can be injected to obtain more analyte mass.

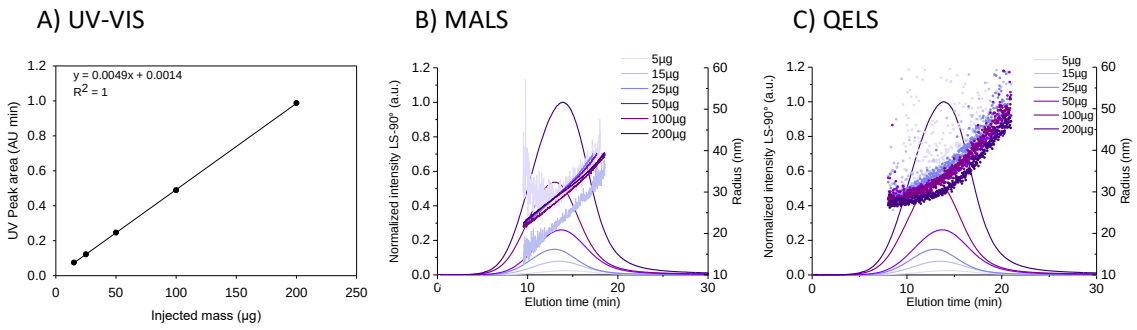

Figure 7: *Injected mass series. Test of the effect of Dox1 injected mass from (5 to 200) µg. A) UV-VIS linear response at 280 nm reporting the area of the elution peak as a function of the injected mass B) Fractograms (normalized excess Rayleigh ratio at 90°), and calculated R_g (line) from the MALS detector and C) R_h (dots) measured by the QELS detector. The shift from light to dark purple represents the increase of injected mass.*

3.3 MD-AF4 optimized method summary

The liposome formulation should first be diluted in the mobile phase to a lipid concentration of 1 mg/mL and stored refrigerated until needed for analysis; the dilution factor will depend on the native concentration, but for the liposomes used in this study it ranged from 15x to 20x. The optimized fractionation method derived from the previously described results consists of an 8 min focus step at FF=2.0, followed by elution with a constant XF=0.3 applied for 45 min with a DF=0.5 and a final elution without XF for 15 min, as summarized in Table 1. The trapezoidal long channel (Wyatt or Postnova) is equipped with a 10 kDa RC membrane and a spacer of 350 µm with medium width. A lipid mass of 25 µg is injected. To minimize potential memory or contamination effects, a washing step between each liposome analysis is conducted. In the washing procedure, 50 µL of PBS mobile phase is injected with an 8 min focus step at a flow rate of 2.0, followed by a 13 min elution without XF at DF=0.5, as described in SI Section 4. The injection volume for washing should meet or exceed the injection volume used for samples.

Table 1: Optimized AF4 fractionation method for liposomal formulations

Channel parameters	**Channel length**	**Long channel (280mm)**	
	Spacer	350 µm medium width	
Membrane	Type	Regenerated cellulose (RC)	
	MWCO	10 kDa	
Flow rates	Injection flow	0.2 mL/min	
	Channel flow	0.5 mL/min	
	Focus flow	2 mL/min	
	Cross flow	0.3 mL/min	
Sample loading	Injection amount	25 µg	
Time and flows parameters (as sequenced in the method)	**Mode**	**Step duration (min)**	**XF (mL/min)**
	(1) Elution	2	0
	(2) Focus	2	-

	(3) Focus + Injection	8	-
	(4) Elution	45	0.3
	(5) Elution	15	0

3.4 Method precision, reproducibility and variability

Method precision was evaluated under repeatability conditions (same analyst, same instrument, same location, same day), by analyzing at least 3 replicate injections of Dox1 in each of three laboratories (see SI Section 1 for detailed description of instrumentation used in each laboratory). The calculated means and standard deviations are summarized in Table 2, while representative fractograms are shown in Figure 8 (Fig. S6). The coefficient of variation (COV) of the repeatability inside each lab does not exceed 5 % for any relevant parameter including recovery, t_R and the calculated size, demonstrating excellent repeatability for the method on all platforms involved in this study. The COV for R is relatively high, due principally to variations in t_0 and the very low ratios measured in this study ($0.02 < R < 0.04$). A low ratio is indicative of a highly efficient fractionation, where the optimal range is approximately $0.03 \leq R \leq 0.2$ [43]. Due to the significant effect of the variation of the void time on R, the value of R was not considered a key parameter for the evaluation of method precision or reproducibility, but the low values are indicating overall of efficient fractionation.

Reproducibility was assessed by applying the method for Dox1, from sample preparation through measurement and data analysis, at three independent facilities using three different AF4 instrument platforms (see SI Section 1 for details) and analysts. The mean and COV values for all endpoints are summarized in Table 2, and demonstrate the excellent repeatability obtained within labs and the very good reproducibility obtained between labs and platforms. For most measurands, such as R%, t_R and R_g the COV is less than 5 %. The COVs for reproducibility of R_h and of R_g/R_h are estimated to be 6.5 % and 9 %, respectively, suggesting that the different online DLS instrumental configurations (e.g., angle, acquisition time, online cell volume) and the different data analysis approaches (single exponential vs. cumulants analysis of the measured correlation function) are significant sources of bias for online determination of R_h.

Finally, the principal factors impacting variability in fractionation of liposomal drug formulations are summarized schematically in a cause and effect diagram (Fig. 9). These factors can be grouped into six components of the measurement process, namely the channel, mobile phase, sample, focus/relaxation, elution and instrument hardware. Of these, only the first five are considered adjustable or selectable by the analyst. The last one, hardware, is dependent on the correct operation of the instrument components according to the manufacturer's specifications. Variations, fluctuations, errors or operational misfunction of any of these factors can contribute to poor quality and/or variability in the fractionation process and results. Tracking the cause of variability or poor performance is

often a matter of trial and error, though following the guidelines set out in ISO TS 21362, Gigault et al 2014 [43] and the optimization process described above can accelerate the process.

Table 2: *Repeatability and reproducibility of the optimized method applied to Dox1. R_h measured by QELS (Wyatt) at scattering angles of 99.9º (Lab1) or 134º (Lab2) or by Zetasizer (Malvern) in flow mode at 173º (Lab3). The mean COV of at least 3 replicate injections is reported for each parameter. For size, the FWHM mean and spread is reported.*

Platform	Replicates	*R*% (%)	t_R (min)	R_g (nm)	R_g Spread (nm)	R_h (nm)	R_h Spread (nm)	R_g/R_h
Lab1	5	98 (1)	11.9 (2.5%)	28.9 (1%)	11.9 (5%)	34.2 (1%)	11.0 (5%)	0.84 (2%)
Lab2	3	95 (1)	13.1 (3.8%)	30.2 (1%)	11.8 (2%)	35.9 (0.5%)	11.3 (4%)	0.83 (4%)
Lab3	3	96 (1)	12.7 (1%)	27.6 (1%)	11.7 (4%)	38.9 (0.5%)	11.7 (5%)	0.71 (3%)
All mean	11	96	12.6	28.9	11.8	36.3	11.3	0.79
All COV		2%	4.8%	4.5%	1%	6.5%	3%	9%

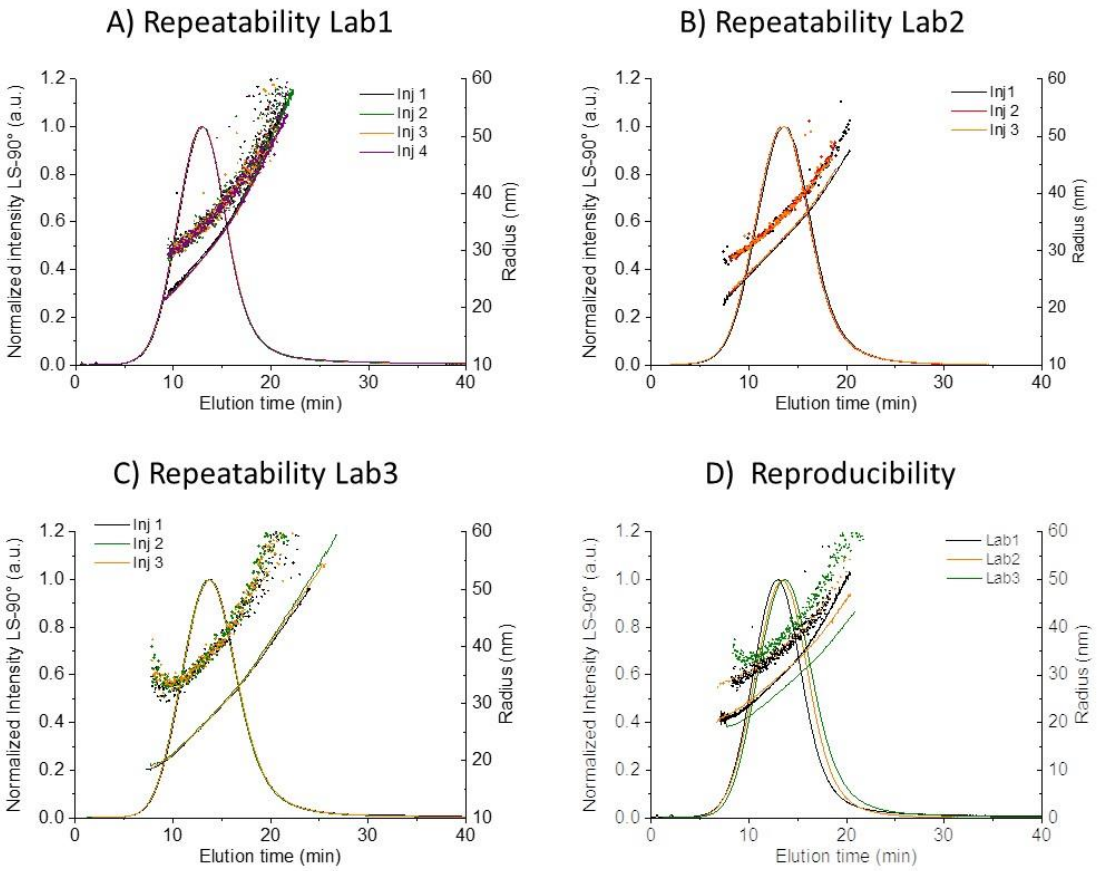

Figure 8: *Repeatability and Reproducibility of the Optimized method for Dox1. Fractograms (normalized excess Rayleigh ratio at 90°), Rg (line) and Rh (dots) for replicate Dox1 injections using the same method on different platforms and labs. Repeatability of A) four replicate injections performed by Lab1 (Wyatt Eclipse Dualtec), B) four replicate injections performed by Lab2 (Wyatt Eclipse 4), C) three replicate injections performed by Lab3 (Postnova AF2000) and D) reproducibility of the optimized method, comparing a single injection by Lab1 (black), Lab2 (orange) and Lab3 (green).*

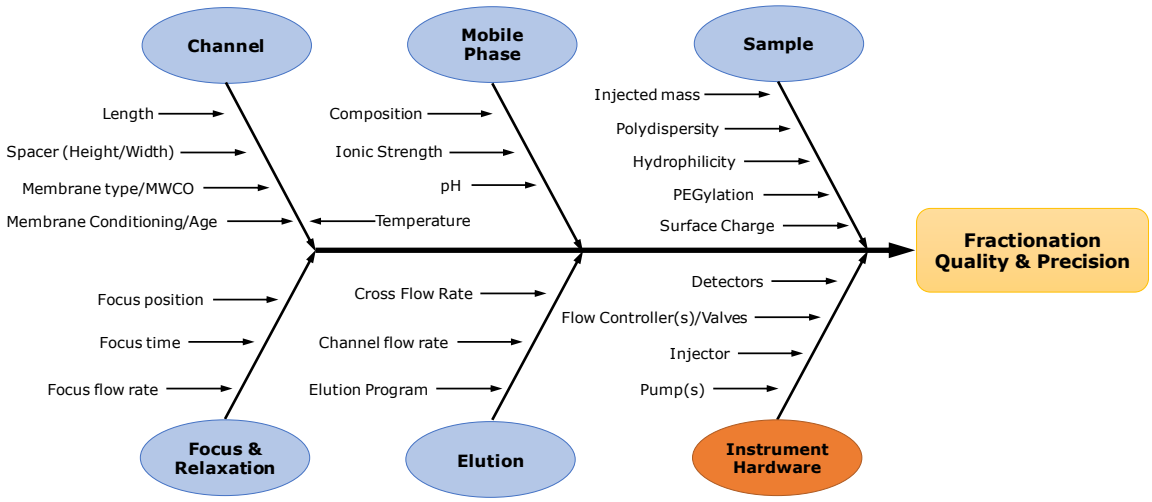

Figure 9: *Cause and effect diagram showing the principal components of fractionation quality and variability for the analysis of liposomal drug formulations. Membrane age refers to effects that appear over time and repeated use of the same membrane, whereas conditioning refers to pretreatment with sample or other complex media prior to analyte injection.*

3.5 Method validation

3.5.1 Polydisperse liposomal formulation

This phase of validation challenged the method using a polydisperse/multimodal research-grade doxorubicin HCl-liposomal formulation (Dox2), one that presents a substantially more complex sample with physical characteristics substantially different from the reference listed drug, but with a composition that is nominally the same. Screening with batch mode DLS indicated a PI of 0.26 (Fig. 10 and Table S4) compared with < 0.05 for Dox1. The MD-AF4 analysis of Dox2 (Fig. 10) shows that the sample contains at least three populations (and possibly four) that were not resolved by batch mode DLS. The first two eluted peaks are associated with spherical vesicles (Peak 1 mode R_g=20 nm, Peak 2 mode R_g=36 nm). A prominent third population eluting after removal of the XF (i.e., the "retained peak" eluting after 45 min), is characterized by a mixture of coeluting, very large entities, and based on initial cryo-TEM results (data not shown), appears to contain predominantly elongated narrow dark objects that resemble free crystals of doxorubicin HCl. Further work would be necessary to confirm this. One could extend the elution run in

this case to fully elute this retained material if desired. Additionally, there is a broad shoulder centered near 30 min, that could represent a forth population, though poorly defined at best.

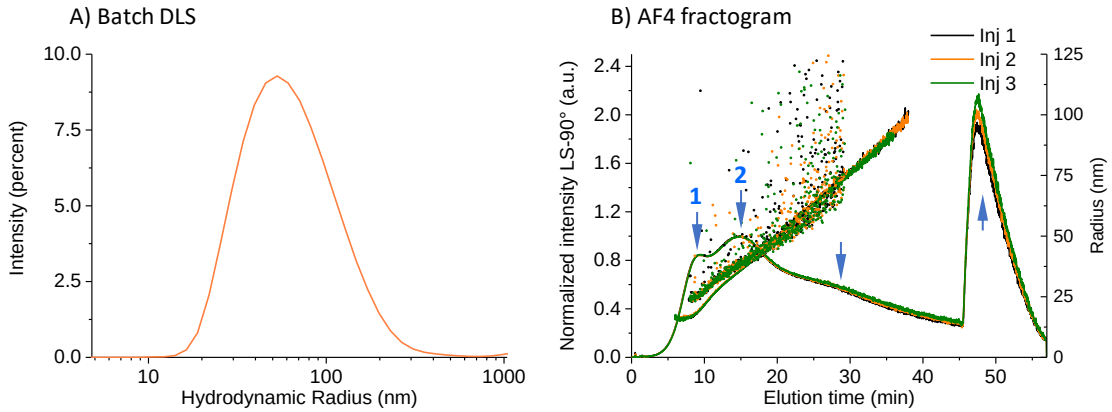

Figure 10: *Dox2: Batch DLS vs AF4 analysis using the optimized method. A) Batch DLS of Dox 2, B) Fractograms showing the elution profile of three replicate injections (normalized excess Rayleigh ratio at 90°), R_g (line) and R_h (dots)versus elution time after injecting 25 µg of Dox2. Blue arrows indicate identifiable component populations.*

Overall, the optimized method offers flexibility to capture the polydispersity, multimodal state and other subtle but possibly important characteristics of this complex liposomal sample. To evaluate the sensitivity of the sample response (e.g., resolution, peak quality, detector signal, recovery) to variations in key method parameters, we examined the effects of elution program, channel spacer, focusing time and injected mass. These results are shown graphically in Fig. S4 and summarized below. The effect of elution (XF) programming and spacer thickness had the greatest impact on the polydisperse Dox2. Specifically, as with the monomodal liposomes, a constant XF is most efficient. The overall fractionation quality changes much more drastically (relative to Dox1) with a change in spacer thickness (350 µm shows the best results). Reducing the focusing time or FF did not improve mass recovery for Dox2, nor did it reduce the size of the retained peak (Fig. S4). This reinforces the conclusion that the retained peak is not an artefact induced during the focusing and relaxation phase, but a population of objects characterized by different physical properties and highlight the capability of the method to answer various liposome related questions. Most notably, the effect of injected mass on the MALS and QELS response (Fig. S5 and Table S18) data suggests that this parameter might need to be modified for polydisperse samples in order to improve the data quality (signal).

Critical Point – For a monomodal sample the analyte mass is concentrated in a relatively narrow band, whereas with a polydisperse sample the mass is widely dispersed as a result of which the detector sensitivity is reduced locally. The injected mass of polydisperse samples can be adjusted, if necessary, to obtain an acceptable signal for data analysis across all components.

Examination of injected mass over the range from (15 to 200) µg showed a pronounced memory effect for Dox2 in the channel (despite the use of a washing step between injections (SI Section 4)). An injected mass of 25 µg produced the best compromise between signal quality and memory effect.

Overall it was demonstrated that the MD-AF4 method optimized for Dox1 was also appropriate to analyze more complex liposomal samples, such as Dox2. Again, repeatability under the optimized method was excellent (Tables S18 and S19, Fig S6).

3.5.2 Generic Doxil formulations

The method has been demonstrated to be precise and reproducible for the prototype doxorubicin HCl-PEG/liposomal formulation Dox1 (identical to the FDA reference listed drug, Doxil®) and its drug-free control Dox1C (see e.g., Fig. S7). To further validate the method, applicability to two FDA approved generics of the reference listed drug (identified as Dox3 and Dox4) was assessed. Representative fractograms for Dox3 and Dox4 are shown and compared with Dox1 in Figure 11. The method performs well with excellent recoveries (> 90%) and repeatability for the two FDA approved generics. Moreover, the approach yields results for the generics that are consistently similar to Dox1, with very small shifts in retention time (see Table S19). Like Dox1, Dox3 and Dox4 are characterized by a single population of spherical vesicles eluting at retention time 12 min with a very small void peak indicating no significant unretained analyte. Dox1 and the generics yield mean R_g (Berry model) and R_h (QELS, 99.9º) values near 30 nm and 35 nm, respectively. The size spread for all three Dox samples is roughly 10 nm and the shape factor falls between 0.84 and 0.86. As with Dox1, for the generics the COV does not exceed 5 % for any relevant parameter, demonstrating excellent within-lab precision for multiple related liposomal products. The repeatability under the optimized method for the two generic Doxil formulations was excellent (Fig. S6).

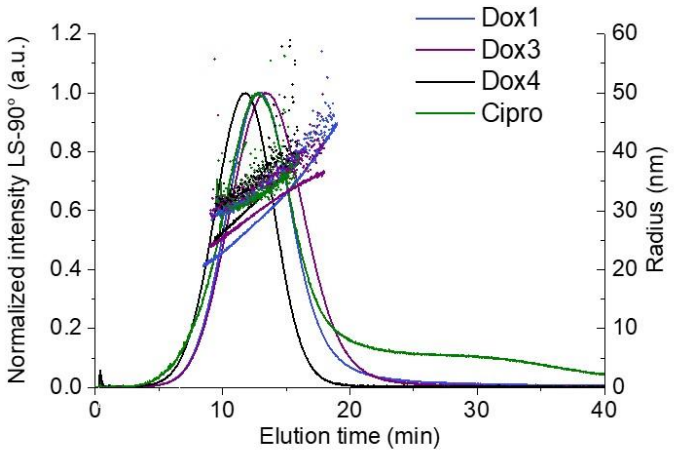

Figure 11: *Application of the optimized method to liposomal formulations. Comparison of the representative fractograms (normalized excess Rayleigh ratio at 90°), R_g (line) and R_h (dots) obtained for Dox1 (violet), Dox3 (purple), and Dox4 (black). and Cipro (green).*

3.5.3 Liposomal ciprofloxacin

Further validation of the method was demonstrated by application to a research-grade PEGylated liposomal antibiotic drug identified here as Cipro (PEGylated hydrogenated soybean phosphatidylcholine liposomal ciprofloxacin). Like Dox1, Cipro is also characterized by a monomodal population with a mean R_g at 32 nm (Fig. 11). The shape factor for Cipro (Table S19) is slightly higher approaching the theoretical value (1) for hollow spheres (0.93 vs. 0.84-0.88 for Dox1, Dox2 and Dox3), suggesting that the Cipro liposomes might possess a less dense core than Dox liposomes. Cipro also shows a lingering tail at longer elution times. Beyond these details, the results again demonstrate that the optimized method is widely applicable for PEGylated liposomal formulations in the nanosize range. Large liposomes ($2R_h$ > 200 nm) will be retained and will elute as a distorted peak following the removal of XF. These larger particles also produce unreliable DLS results online, even at relatively low DF. The repeatability under the optimized method was excellent (Fig. S6).

3.5.4 Application in complex media

As recently reported by the FDA [46], when NEPs are evaluated, in addition to characterizing the physico-chemical properties of the analyte, in order to fully assess their quality, safety and efficacy profile it is also necessary to measure their stability and interactions in complex protein-containing biological media. In fact, when NEPs are entering the systemic circulation system, the interaction of plasma proteins with their surface may endow NEP systems with new properties, e.g. modifying their surface (formation of protein corona), size (formation of corona, agglomeration, dissolution) and drug delivery (impact drug release). The investigation of size stability in complex biological media is a difficult challenge that requires the use of high-resolution techniques [12]. MD-AF4 is a very powerful method to measure NEP-protein interactions, thanks to the separation of free proteins from the analyte particles prior to analysis. This has previously been demonstrated for liposomal samples [22] and lipid-based nanoparticles [28].

Herein the capacity of the optimized MD-AF4 method to analyse the size of Dox1 and Dox2 in the presence of serum proteins was evaluated. For this purpose, the liposomal formulations were diluted into 10 % buffered fetal bovine serum (FBS), and immediately analysed using the optimized method without further incubation.

The results for the fractionation of liposomal doxorubicin samples Dox1 and Dox2 in simple and complex media are reported in Figure 12 and Table S20. The optimized elution program successfully separates free protein (see control fractogram of buffered FBS in yellow) from the liposome component. Under the conditions tested, the fractograms of the

liposomes observed following dilution into 10 % FBS are phenomenologically similar to the liposomes without protein-containing FBS (i.e., the same principle features appear at roughly the same elution times). Overall, we can conclude that the optimized MD-AF4 method has the potential to analyse liposomal samples in complex biological media as well as simple PBS.

Critical point: This experiment provides proof of principle, while actual preclinical studies of liposomal drug interactions in complex media should include appropriate incubation periods prior to analysis.

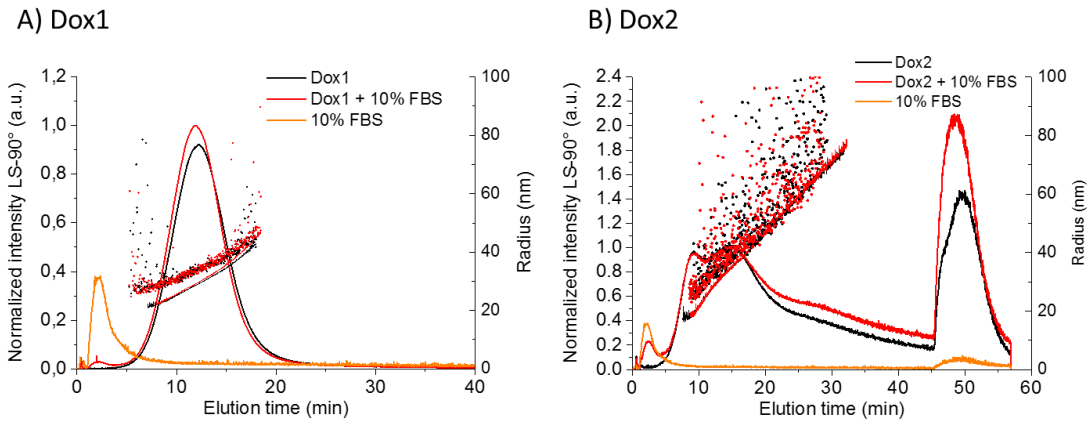

Figure 12: *Measurement of Dox1 and Dox2 in complex media. AF4 fractograms (normalized excess Rayleigh ratio at 90°), the R_g (line) and R_h (dots) versus elution time by injecting A) Dox1 and B) Dox2 with (red) and without (black) 10 % FBS. Orange fractogram is the PBS + 10% FBS control.*

3.6 Method limitations and troubleshooting

The method described here should work well with any PEGylated liposomal drug formulation as well as their controls (empty liposomes). Liposomes that do not contain PEG in their outer shell may exhibit stability issues and/or substantial membrane interactions in the AF4 channel. These materials should be evaluated on a case-by-case basis. But generally, any liposome that has a hydrophilic, negatively charged or neutral, external surface and is stable in PBS or saline, should be applicable.

As stated previously, online DLS measurements have limitations with respect to the upper size range, especially at relatively high DF values. This limitation is most evident in the standard MALS cell and less so in the type of cell used with a Zetasizer in flow-mode operation. A larger bore MALS cell can mitigate this limitation for particles larger than about 75 nm (radius). The root mean square radius is limited on the low end to about 10 nm, but this limit is a function of the laser wavelength and angular range available on a specific system. The upper limit for R_g is well beyond the size range of interest for this method. We strongly suggest the analyst confirm the applicable size range for each specific online detector configuration by analysing size standards or quality control materials, and to avoid reporting size values outside of this range.

Highly polydisperse or multimodal samples present the greatest challenge for application of this method. But as demonstrated with Dox2, the method is sufficiently flexible to capture basic information regarding the physical state of complex analytes. Simple adjustments, such as using a longer elution time, can be made within the scope of this method in order to ensure that all components are fractionated and analysed. Samples containing very large liposomes or liposome products (e.g., agglomerates) greater than about 200 nm radius, are outside the scope of this method and its intended application to drug formulations.

Low mass recovery (less than 90 % for PEGylated liposomes) indicates that the analyte is interacting strongly with the membrane (accumulation wall), though losses can also occur at other surfaces in contact with the fluid sample. Reducing FF, focus time and XF during elution can improve recovery. However, very low recoveries (< 70 %) that cannot be improved by the usual approach most likely disqualify the sample as incompatible with the method, and further suggest that the material properties are inappropriate for clinical applications. An unexpected low recovery for a formulation that has proven highly recoverable in the past is a red flag suggesting a change has occurred as a result of, for example, aging, storage, or a manufacturing quality control.

Critical point – An alternative approach to improve recovery for high-loss analytes is to passivate the membrane with a suitable coating such as a surfactant or protein. Use of passivation must be validated as part of the overall method performance.

Low or noisy detector response can usually be addressed by increasing the injected analyte mass. Low or noisy signals might occur, for instance, in a polydisperse sample where the mass is spread out over a larger elution time. If increasing the injection mass does not eliminate the problem, the detector itself should be evaluated or the cell cleaned and retested. On the other hand, a high MALS baseline signal suggests the cell is fouled and requires cleaning. Comparison with a known quality control material such as PSL is recommended.

Memory effects occur when components from a previously injected sample elute during a new injection. The most likely cause is material adhering to the membrane or other surfaces, then releasing during the second elution. If the memory effect is substantial (i.e., it significantly interferes with the outcome of an analysis), there are steps that can be taken to eliminate or minimize the effect. In the present work, the method includes a mobile phase injection (without cross flow) before each sample injection. This approach can be extended if necessary. For instance, multiple mobile phase injections could be performed prior to each sample injection. Memory effects are usually associated with recovery issues, so improving recovery can help eliminate memory effects.

Critical point – The results obtain with the washing step has to be verified before starting another experiment. In the case of the presence of sufficient materials, a second washing step run has to be conducted and checked.

Best Practice Note – The lifetime of a membrane depends on the number of injections, the time over which analyses are performed, the duration of the washing/elution steps, and the quantity of mass injected per analysis. Taking all factors into consideration, a membrane can typically be used for 30-50 analyses of liposomal samples before replacement is necessary. This number can vary widely for different types of samples and experimental conditions. If memory effects persist after several washing cycles, then the membrane should be replaced.

The analyst should always monitor channel pressure at all stages of the experiment and look for any unexpected changes in pressure (typically increases). The system should automatically terminate an experiment if the pressure exceeds the manufacturer's stated operational range. But any sudden or unexpected increase in pressure should be investigated immediately. The cause can range from a clogged membrane or fluid line to a bad valve or flow controller.

Summary and Conclusions

In this extensive multi-laboratory investigation, we evaluated a broad range of instrument parameters and experimental factors that influence the outcome of multi-detector asymmetrical-flow field flow fractionation (MD-AF4) applied to the physical characterization of nanometric liposomal drug formulations. Liposomal doxorubicin HCl was utilized as the prototypical test material for this study. The principal outcome of this work is an optimized MD-AF4-based method (schematically illustrated in Fig. 13) validated across different instrument platforms, three laboratories, multiple drug formulations and in complex media containing serum proteins. The method was evaluated for a research grade form of the reference listed drug Doxil, a research grade polydisperse formulation, two pharmaceutical generics of Doxil and a research grade ciprofloxacin liposome. All test materials were PEGylated.

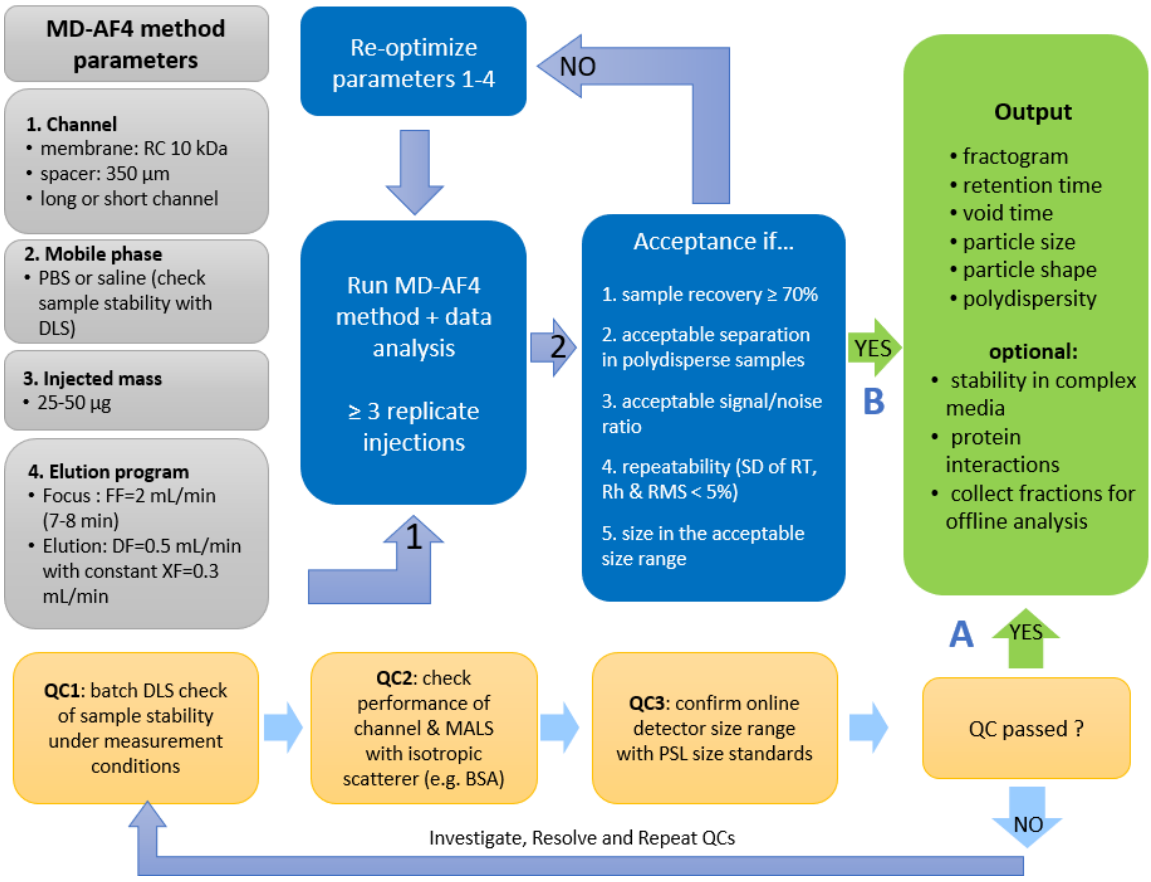

Figure 13: *Work flow chart showing principal steps in MD-AF4 method application. Both quality control (A) and fractionation/analysis results (B) must yield green arrows to meet overall method acceptance criteria, with QC preceding sample analysis.*

Key parameters and factors were identified and optimized in order to yield reliable and accurate results with respect to fractionation quality, particle size and size distribution, particle shape, recovery, separation efficiency and selectivity. Interlaboratory reproducibility and intralaboratory precision were evaluated. The resulting method proved efficient and sufficiently flexible to tackle a range of physical states and formulations. We observed that small variations in phosphate buffered saline composition (common in commercial products) did not significantly impact results, and that formulations can be analysed in complex media without detriment to the outcome. In fact, results show that this method has the potential to provide additional information regarding interactions between the drug and medium components such as serum proteins. Additionally, the potential for quantifying and discriminating between encapsulated and free drug using MD-AF4, coincidentally with analysis of the physical state of the drug, is proposed and under further investigation.

This method meets a documented high priority need in regulatory science as applied to nano-enabled medical products, and has substantial advantages over commonly used batch

dynamic light scattering (DLS), particularly in the case of polydisperse and multimodal complex formulations, where DLS results can be both misleading and difficult to interpret. In addition to liposomal formulations, we believe the method can be easily adapted to the measurement of other NEPs (such as lipid nanoparticles).

Overall, this optimized method will help accelerate development of NEPS, and facilitate their regulatory review, ultimately leading to faster translation of innovative concepts from the bench to the clinic. This method will form the basis for a future international consensus test method, that will involve a more extensive interlaboratory comparison. Additionally, the approach used in this work (based on international collaboration between leading non-regulatory institutions) can be replicated to address other identified gaps in the analytical characterization of various classes of NEPs.

Acknowledgements

The contributions of JP were funded in part by NIST grant No.70NANB17H250. This research was in part funded by the project EUNCL 2015, a European Union's Horizon 2020 Research and Innovation Program under grant agreement No. 654190. The instrumentation used in Lab2 is part of the NanoID platform that was supported by the French Investissement d'Avenir ANR-10- EQPX-39. Pharmaceutical generics were obtained with the help of Dr. Amy Barton Pai, University of Michigan College of Pharmacy. The authors thank Tae Joon Cho (NIST) and Jeff Clogston (NCI/NCL) for manuscript review and helpful comments. The authors also gratefully acknowledge timely input and support from Postnova Analytics and Wyatt Technology during the execution of this study. Finally, this work was conducted under the auspices of the ad hoc EU-US Nanomedicine Collaboratory.

Abbreviation list

AF4 = asymmetrical-flow field flow fractionation
DF = channel flow or detector flow rate
DLS = dynamic light scattering
EMA = European Medicines Agency
FBS = fetal bovine serum
FDA = US Food and Drug Administration
FF = focus flow rate
FWHM = full width at half maximum
MALS = multi-angle light scattering
MD = multi detector
NEP = nanotechnology enabled pharmaceutical
NIST = National Institute of Standards and Technology
NNLS = non-negative constrained least squares analysis
PBS = phosphate buffered saline

PI = polydispersity index
PES = polyethersulfone
PSL =polystyrene nanosphere
QELS = quasi-elastic light scattering
RC = regenerated cellulose
R_h = hydrodynamic radius
R_g = root mean square radius
R = retention ratio ($=t_0/t_R$)
R% = estimated mass recovery
t_R = retention time
t_0= void time
XF = cross flow rate
z-avg = z-average; mean hydrodynamic diameter calculated by cumulants analysis

REFERENCES

[1] A.C. Anselmo, S. Mitragotri, Nanoparticles in the clinic, Bioengineering & translational medicine, 1 (2016) 10-29.

[2] S.R. D'Mello, C.N. Cruz, M.-L. Chen, M. Kapoor, S.L. Lee, K.M. Tyner, The evolving landscape of drug products containing nanomaterials in the United States, Nat Nano, 12 (2017) 523-529.

[3] O.C. Farokhzad, R. Langer, Impact of nanotechnology on drug delivery, ACS nano, 3 (2009) 16-20.

[4] D. Myshko, Nanotechnology: It's a Small World, PharmaVOICE, (2004).

[5] K. Park, The beginning of the end of the nanomedicine hype, in, 2019.

[6] P. Grodzinski, NCI Centers of Cancer Nanotechnology Excellence (CCNEs) - A full story to set the record straight, J Control Release, (2019).

[7] A.M. Cryer, A.J. Thorley, Nanotechnology in the diagnosis and treatment of lung cancer, Pharmacology & therapeutics, 198 (2019) 189-205.

[8] T.J. Anchordoquy, Y. Barenholz, D. Boraschi, M. Chorny, P. Decuzzi, M.A. Dobrovolskaia, Z.S. Farhangrazi, D. Farrell, A. Gabizon, H. Ghandehari, Mechanisms and barriers in cancer nanomedicine: addressing challenges, looking for solutions, in, ACS Publications, 2017.

[9] J.H. Grossman, R.M. Crist, J.D. Clogston, Early Development Challenges for Drug Products Containing Nanomaterials, The AAPS Journal, 19 (2017) 92-102.

[10] M. Swierczewska, R.M. Crist, S.E. McNeil, Evaluating Nanomedicines: Obstacles and Advancements, in: Characterization of Nanoparticles Intended for Drug Delivery, Springer, 2018, pp. 3-16.

[11] K.M. Tyner, P. Zou, X. Yang, H. Zhang, C.N. Cruz, S.L. Lee, Product quality for nanomaterials: current US experience and perspective, Wiley Interdisciplinary Reviews: Nanomedicine and Nanobiotechnology, 7 (2015) 640-654.

[12] S. Gioria, F. Caputo, P. Urbán, C.M. Maguire, S. Bremer-Hoffmann, A. Prina-Mello, L. Calzolai, D. Mehn, Are existing standard methods suitable for the evaluation of nanomedicines: some case studies, Nanomedicine, 13 (2018) 539-554.

[13] B. Halamoda-Kenzaoui, S. Baconnier, T. Bastogne, D. Bazile, P. Boisseau, G. Borchard, S.E. Borgos, L. Calzolai, K. Cederbrant, G. Di Felice, Bridging communities in the field of nanomedicine, Regulatory Toxicology and Pharmacology, 106 (2019) 187-196.

[14] S. Bremer-Hoffmann, B. Halamoda-Kenzaoui, S.E. Borgos, Identification of regulatory needs for nanomedicines, Journal of Interdisciplinary Nanomedicine, 3 (2018) 4-15.

[15] B. Halamoda-Kenzaoui, U. Holzwarth, G. Roebben, A. Bogni, S. Bremer-Hoffmann, Mapping of the available standards against the regulatory needs for nanomedicines, Wiley Interdisciplinary Reviews: Nanomedicine and Nanobiotechnology, 11 (2019) e1531.

[16] Global Summit on Regulatory Science (GSRS16) Nanotechnology Standards and Applications - Final Report, in, 2016.

[17] U. Food, D. Administration, Liposome Drug Products: Chemistry, Manufacturing, and Controls; Human Pharmacokinetics and Bioavailability; and Labeling Documentation. Guidance for Industry, Guidance for Industry, (2018).

[18] L. Calzolai, D. Gilliland, C.P. Garcìa, F. Rossi, Separation and characterization of gold nanoparticle mixtures by flow-field-flow fractionation, Journal of Chromatography A, 1218 (2011) 4234-4239.

[19] D. Mehn, F. Caputo, M. Rösslein, L. Calzolai, F. Saint-Antonin, T. Courant, P. Wick, D. Gilliland, Larger or more? Nanoparticle characterisation methods for recognition of dimers, RSC Advances, 7 (2017) 27747-27754.
[20] F. Caputo, A. Arnould, M. Bacia, W.L. Ling, E. Rustique, I. Texier, A.P. Mello, A.-C. Couffin, Measuring Particle Size Distribution by Asymmetric Flow Field Flow Fractionation: A Powerful Method for the Preclinical Characterization of Lipid-Based Nanoparticles, Molecular pharmaceutics, 16 (2019) 756-767.
[21] F. Caputo, J. Clogston, L. Calzolai, M. Rösslein, A. Prina-Mello, Measuring particle size distribution of nanoparticle enabled medicinal products, the joint view of EUNCL and NCI-NCL. A step by step approach combining orthogonal measurements with increasing complexity, Journal of Controlled Release, (2019).
[22] D. Mehn, F. Caputo, M. Rösslein, EUNCLPCC-022. - Measurement of Particle Size Distribution of Protein Binding, of Mean Molecular Weight of Polymeric NP Components, Study of Batch to Batch Reproducibility, and Study of Release of Free Coating from NP Surface by FFF-MALS, in, 2017.
[23] M. Marioli, W.T. Kok, Recovery, overloading, and protein interactions in asymmetrical flow field-flow fractionation, Analytical and bioanalytical chemistry, 411 (2019) 2327-2338.
[24] M. Wagner, S. Holzschuh, A. Traeger, A. Fahr, U.S. Schubert, Asymmetric flow field-flow fractionation in the field of nanomedicine, Analytical chemistry, 86 (2014) 5201-5210.
[25] C. Contado, Field flow fractionation techniques to explore the "nano-world", Analytical and bioanalytical chemistry, 409 (2017) 2501-2518.
[26] J. Kuntsche, C. Decker, A. Fahr, Analysis of liposomes using asymmetrical flow field-flow fractionation: Separation conditions and drug/lipid recovery, Journal of Separation Science, 35 (2012) 1993-2001.
[27] P. Iavicoli, P. Urbán, A. Bella, M.G. Ryadnov, F. Rossi, L. Calzolai, Application of asymmetric flow field-flow fractionation hyphenations for liposome–antimicrobial peptide interaction, Journal of Chromatography A, 1422 (2015) 260-269.
[28] S. Hupfeld, D. Ausbacher, M. Brandl, Asymmetric flow field-flow fractionation of liposomes: 2. Concentration detection and adsorptive loss phenomena, Journal of separation science, 32 (2009) 3555-3561.
[29] A. Hinna, F. Steiniger, S. Hupfeld, M. Brandl, J. Kuntsche, Asymmetrical flow field-flow fractionation with on-line detection for drug transfer studies: a feasibility study, Analytical and Bioanalytical Chemistry, 406 (2014) 7827-7839.
[30] D. Van Haute, W. Jiang, T. Mudalige, Evaluation of size-based distribution of drug and excipient in amphotericin B liposomal formulation, International journal of pharmaceutics, 569 (2019) 118603.
[31] S. Hupfeld, H.H. Moen, D. Ausbacher, H. Haas, M. Brandl, Liposome fractionation and size analysis by asymmetrical flow field-flow fractionation/multi-angle light scattering: influence of ionic strength and osmotic pressure of the carrier liquid, Chemistry and physics of lipids, 163 (2010) 141-147.
[32] L.O. Monteiro, A.n. Malachias, G. Pound-Lana, R.r. Magalhães-Paniago, V.C. Mosqueira, M.n.C. Oliveira, A.L.s.B. de Barros, E.A. Leite, Paclitaxel-loaded pH-sensitive liposome: new insights on structural and physicochemical characterization, Langmuir, 34 (2018) 5728-5737.

[33] T.J. Evjen, S. Hupfeld, S. Barnert, S. Fossheim, R. Schubert, M. Brandl, Physicochemical characterization of liposomes after ultrasound exposure – Mechanisms of drug release, Journal of Pharmaceutical and Biomedical Analysis, 78-79 (2013) 118-122.
[34] H. Zhang, D. Freitas, H.S. Kim, K. Fabijanic, Z. Li, H. Chen, M.T. Mark, H. Molina, A.B. Martin, L. Bojmar, J. Fang, S. Rampersaud, A. Hoshino, I. Matei, C.M. Kenific, M. Nakajima, A.P. Mutvei, P. Sansone, W. Buehring, H. Wang, J.P. Jimenez, L. Cohen-Gould, N. Paknejad, M. Brendel, K. Manova-Todorova, A. Magalhães, J.A. Ferreira, H. Osório, A.M. Silva, A. Massey, J.R. Cubillos-Ruiz, G. Galletti, P. Giannakakou, A.M. Cuervo, J. Blenis, R. Schwartz, M.S. Brady, H. Peinado, J. Bromberg, H. Matsui, C.A. Reis, D. Lyden, Identification of distinct nanoparticles and subsets of extracellular vesicles by asymmetric flow field-flow fractionation, Nature Cell Biology, 20 (2018) 332-343.
[35] H. Zhang, D. Lyden, A protocol for asymmetric-flow field-flow fractionation (AF4) of small extracellular vesicles, Protocol Exchange, 10 (2018).
[36] Y.C. Barenholz, Doxil®—the first FDA-approved nano-drug: lessons learned, Journal of controlled release, 160 (2012) 117-134.
[37] Y. Bavli, I. Winkler, B.M. Chen, S. Roffler, R. Cohen, J. Szebeni, Y. Barenholz, Doxebo (doxorubicin-free Doxil-like liposomes) is safe to use as a pre-treatment to prevent infusion reactions to PEGylated nanodrugs, Journal of Controlled Release, (2019).
[38] Y.C. Barenholz, Hebrew University Hadassah Medical School, in, Personal Communication, 23 October 2019.
[39] M. Andersson, B. Wittgren, K.-G. Wahlund, Accuracy in multiangle light scattering measurements for molar mass and radius estimations. Model calculations and experiments, Analytical Chemistry, 75 (2003) 4279-4291.
[40] P.J. Wyatt, Light scattering and the absolute characterization of macromolecules, Analytica chimica acta, 272 (1993) 1-40.
[41] W. Burchard, M. Schmidt, W.H. Stockmayer, Information on Polydispersity and Branching from Combined Quasi-Elastic and Intergrated Scattering, Macromolecules, 13 (1980) 1265-1272.
[42] ISO/TS 21362:2018 - Nanotechnologies — Analysis of nano-objects using asymmetrical-flow and centrifugal field-flow fractionation, in, 2018.
[43] J. Gigault, J.M. Pettibone, C. Schmitt, V.A. Hackley, Rational strategy for characterization of nanoscale particles by asymmetric-flow field flow fractionation: a tutorial, Analytica chimica acta, 809 (2014) 9-24.
[44] S. Sitar, V. Vezočnik, P. Maček, K. Kogej, D. Pahovnik, E. Žagar, Pitfalls in size characterization of soft particles by dynamic light scattering online coupled to asymmetrical flow field-flow fractionation, Analytical chemistry, 89 (2017) 11744-11752.
[45] A. Litzen, K.G. Wahlund, Zone broadening and dilution in rectangular and trapezoidal asymmetrical flow field-flow fractionation channels, Analytical chemistry, 63 (1991) 1001-1007.
[46] FDA/CDER/CBER, Drug Products, Including Biological Products, that Contain NanomaterialsGuidance for Industry in, 2017.

Supplemental Information

Physical characterization of liposomal drug formulations using multi-detector asymmetrical-flow field flow fractionation

Parot, J.[a,b], Caputo, F.[c], Mehn, D.[d], Hackley, V.A.[a], Calzolai, L.[d]

[a] Materials Measurement Science Division, National Institute of Standards and Technology, Gaithersburg, Maryland 20899-8520, USA

[b] Theiss Research, La Jolla, California 92037, USA

[c] Université Grenoble Alpes, CEA, LETI, F-38000 Grenoble, France

[d] European Commission, Joint Research Centre (JRC), Ispra, Italy

1. Instrumental configurations by laboratory

Lab 1: Agilent Technologies (Santa Clara, CA USA)1 1100-series isocratic pump equipped with a Gastorr TG-14 degasser, fan Agilent 1260 ALS autosampler with a 900 µL injection loop connected to a Wyatt Technology Eclipse DualTec AF4 system. On-line detectors include an Agilent 1200 UV-VIS absorbance diode array detector with spectral range (190 to 950) nm (ii) a Wyatt DAWN HELEOS II MALS detector (λ=661 nm) equipped with 18 detectors at angles from 12.8° to 157.8° (table S3), a standard flow cell (1.2mm diameter), a fiber optic based Wyatt on-line quasi-elastic light scattering (QELS) DLS detector installed at a scattering angle of 99.9° (MALS position LS-12) and/or (iii) a Zetasizer Nano ZS (Malvern Panalytical) with a wavelength of 633 nm and operating in flow mode at a scattering angle of 177°. Data analysis was performed with Wyatt ASTRA Version 6.1.7.17 and Zetasizer software for flow DLS.

Lab 2: Agilent 1260-series Infinity Bio-inert Quaternary Pump equipped with an Agilent 1260 Infinity Bio-inert High Performance Autosampler (100µL injection loop) connected to a Wyatt Eclipse AF4 system. On-line detectors include (i) an Agilent 1200 UV-VIS absorbance detector with single wavelength selectable from (190 to 800) nm and (ii) a Wyatt DAWN HELEOS II MALS detector (λ= 664.3 nm), a standard flow cell (1.2mm diameter) and with a Wyatt QELS installed at a scattering angle of 134° (MALS position LS-16). Data analysis was performed with Wyatt ASTRA Version 6.1.2.84.

Lab 3: Postnova AF2000 AF4 system (Postnova Analytics GmbH, Landsberg, Germany) equipped with degasser (Postnova 7520), two isocratic pumps (Postnova 1130), using a manual injection loop of 100 µL. The system uses the following on-line detectors: (i) a UV-VIS detector (Postnova 3212) with single wavelength selectable from 190 nm to 800 nm; (ii) a Postnova 3621 MALS detector (λ=532 nm) equipped with 21 detectors at angles from 7° to 164° (table S3); (iii) Zetasizer Nano ZS (Malvern Panalytical) equipped with flow-mode cell, using a wavelength of 633 nm and

[1] The identification of any commercial product or trade name does not imply endorsement or recommendation by the National Institute of Standards and Technology.

detecting in backscattering at 173°. Data analysis was performed with Postnova data analysis software 2.1.0.5. (AF4-UV-MALS data) and Zetasizer software for flow DLS.

2. Data analysis and reporting

Fractogram presentation

Fractograms are reported by plotting the UV-Vis and/or light scattering intensity at a specific angle (e.g., 90° for MALS, 173° for the Zetasizer) versus the elution time beginning when focus/relaxation ends and detector flow (with or without cross flow) begins. Normalized intensities are extracted as processed by the instrumental software. More detailed information on the light scattering properties of the samples can be obtained in specific situations (e.g., by extracting the unnormalized excess Rayleigh ratio from each MALS angle). Mass recovery, retention time, void time and the retention ratio are obtained using the fractogram trace from the concentration detector (UV-Vis at 280 nm in the method presented here). Retention and void time are determined at the peak maximum. The analyst should report recovery, retention time, void time and retention ratio, in addition to recovery.

Particle size determination

For the purpose of this optimized MD-AF4 method, the Berry model for analysis of MALS data (to obtain the rms radius, R_g) is recommended for the general analysis of liposomal samples, being one of the suggested models to be used over a wide size range (without specific size limitations) when the shape of the particle is not known (no spherical assumption is necessary).

$$\text{Berry plot: } \sqrt{\frac{Kc}{R_\theta}} \text{ vs. } sin^2\left(\frac{\theta}{2}\right)$$

where K is an optical constant, c is the mass concentration of scatterers, R_θ is the excess Rayleigh ratio, and θ is the scattering angle. To obtain R_g only (not molar mass) the Berry plot does not require knowledge of the concentration. Since different models can generate somewhat different results, the approach used in the data analysis should always be reported. MALS data should be analyzed selecting a model based on the knowledge of the analyte (size range, shape if known) and quality of the fit (e.g., by evaluating the fit R^2 value across the peak), and by adjusting the number of MALS angles used in the model based on quality of fit and quality of data at each angle. Based on our experience, we recommend using a minimum of 8 angles for analysis.

The use of a DLS detector provides hydrodynamic size, R_h, during fractionation. For the purpose of this optimized MD-AF4 method, DLS data should be analyzed according to the quality of the fit (e.g., by evaluating the fit error across the peak), the correlation function shape/noise and by adjusting the processing parameters as required. Note that different processes are available to analyze measured correlation data obtained online. For instance, a single exponential fit versus cumulant analysis. The Zetasizer in flow-mode operation uses cumulants analysis, while the QELS detector provides several methods including cumulants and single exponential. In any case, the analysis method should be reported. Theoretically, the single exponential and cumulants analysis should produce similar results for online DLS, since each data slice in the fractogram is essentially monodisperse.

Reporting particle size

In order to calculate and report an average size value (R_g and/or R_h), ISO/TS 21362:2018 suggests that, when a monodispersed or a monomodal sample characterized by a limited polydispersity is measured and a symmetric elution peak is obtained, the mean size value should be calculated by averaging the values across the full width at half maximum (FWHM) (arithmetic mean). On the contrary, when the sample is characterized by a clear upward trend and/or by multiple populations which are not completely resolved, the calculated mean across the FWHM might not represent the true mean size of the particle population. In a similar scenario, we suggest only to plot the size values across the FWHM in the fractogram and to report the mode (peak maximum) values of the detectable peaks.

For all samples the spread value (difference between the minimum and maximum value across the FWHM) can be an indication of the polydispersity of the sample.

The shape factor ($\rho = R_g/R_h$) should be reported in a manner similar to that described above for size values.

3. AF4 PSL elution method

The method used to analyze NIST Traceable PSL spheres consisted of a focus-injection step for 5 min at focus flow 1, followed by elution at detector flow DF=(0.5 or 1) mL/min with an exponentially decaying cross flow from XF=(1 to 0) mL/min for 45 min. The trapezoidal long channel (Wyatt) was equipped with a 10 kDa PES membrane and a 350 µm spacer. The mobile phase was 0.5 mmol/L ammonium nitrate and the injection volume was 10 µL.

Step duration (min)	Mode	XF (mL/min)
2	Elution	0
2	Focus	-
5	Focus + Inject	-
45	Elution	1 to 0
10	Elution	0

4. AF4 between sample washing protocol

100 µL of PBS is injected during a focus-injection step for 8 min at focus flow rate of 2 mL/min, followed by elution at detector flow DF= 0.5 mL/min without cross flow for 13 min. This procedure is repeated after each sample analysis to help ensure that memory effects are minimized and that each sample injection yields consistent results.

Step duration (min)	Mode	cross flow (mL/min)
2	Elution	0
2	Focus	-
8	Focus + Inject	-
13	Elution	0

5. Supplementary figures

Note: all flow rates given in mL/min, XF=cross flow, DF=detector flow.

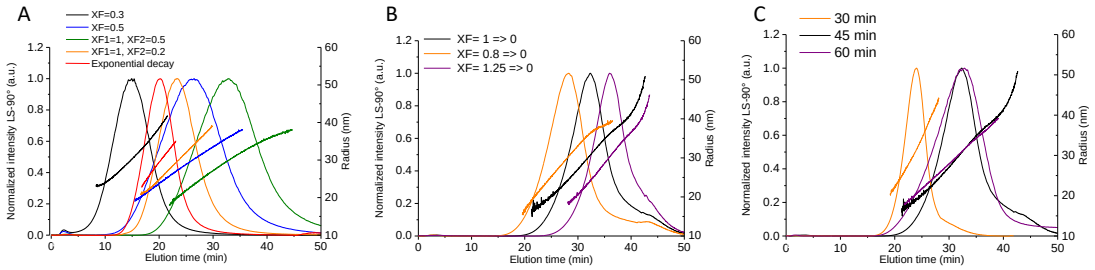

Figure S1: Test of multiple elution programs for Dox1. *AF4 fractograms showing normalized excess Rayleigh ratio at 90° versus elution time with R_g overlaid. Injection of 50 µg Dox1 and applying A) constant cross flow with XF=0.3 or 0.5, two stage cross flow with XF=1 and 0.5 then 1 and 0.3, exponential cross flow decay, B) linear cross flow decay to XF=0 in 45 min (starting XF=0.8, 1, 1.25), C) linear cross flow decay to XF=0 in 30, 45 or 60 min (starting XF= 1 and DF=0.5).*

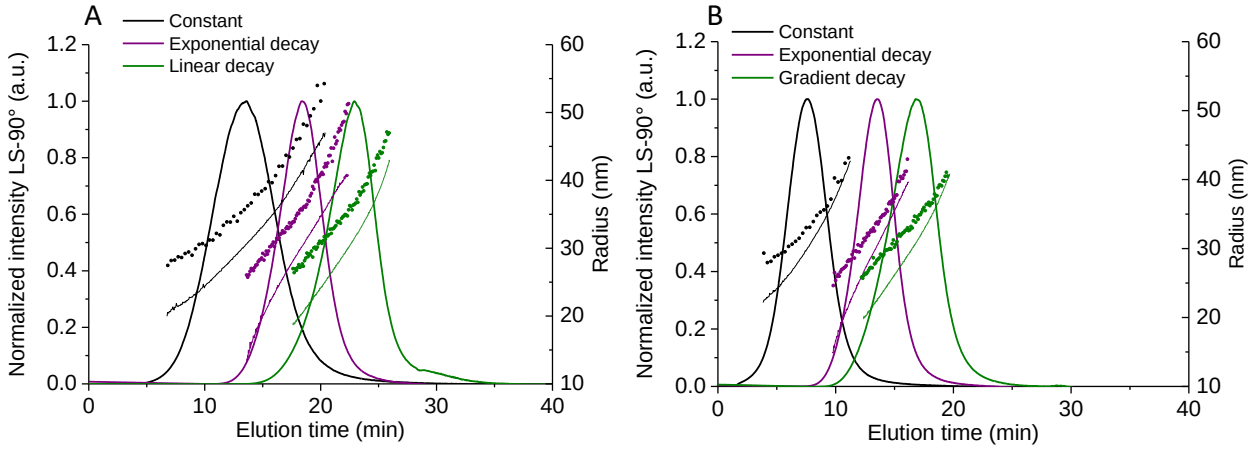

Figure S2: Comparison of three elution methods and DF for Dox1. AF4 fractograms showing normalized excess Rayleigh ratio at 90° versus elution time with R_g (lines) and R_h (dots) overlaid. Injection of 50 µg of Dox1 and applying a constant cross flow XF=0.3 (black), or an exponential decay from XF=1 to XF=0 in 60 min (purple) or a linear decay from XF=1 to XF=0 in 30 min (green) with a DF of A) 0.5 or B) 1.

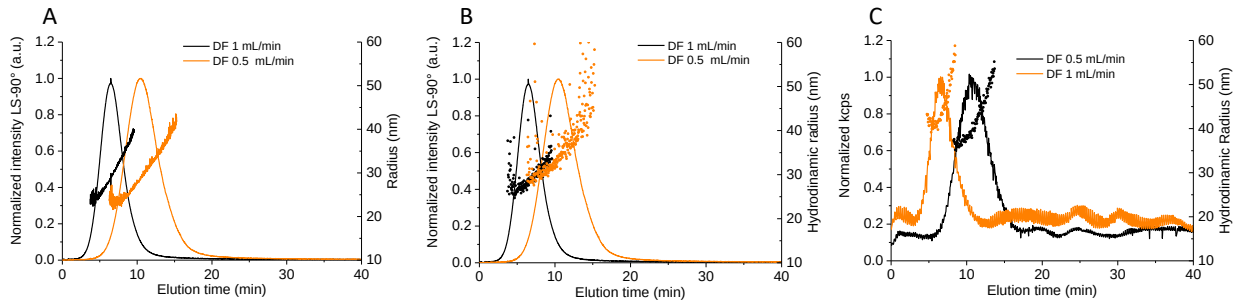

Figure S3: *Measurement of Dox1 using different sizing detectors as measured by Lab1. DF=0.5 (black) and DF=1 (orange). A) AF4 fractograms showing normalized excess Rayleigh ratio at 90° and R_g measured by MALS, B) AF4 fractogram and R_h measured by online DLS (Wyatt QELS) and C) AF4 fractogram (normalized kcps) and hydrodynamic radius R_h measured by online DLS (Malvern Zetasizer).*

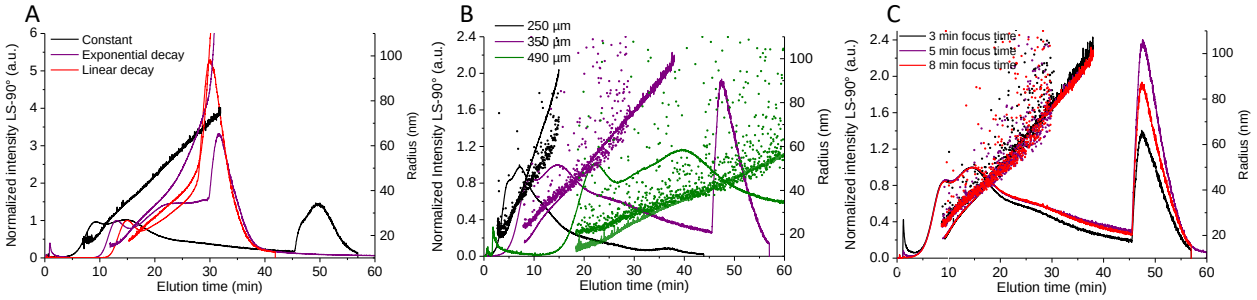

Figure S4: Test of different conditions for Dox2. AF4 fractograms showing normalized excess Rayleigh ratio at 90° versus elution time with R_g (lines) and R_h (dots) for 25 µg injection of Dox2. A) comparison of elution method by applying a constant cross flow XF=0.3 (black), or an exponential decay from XF=1 to XF=0 in 60 min (purple) or a linear decay from XF=1 to XF=0 in 30 min (red). B) effect of channel spacer (black: 250 µm, violet: 350 µm, green: 490 µm) and C) effect of focus time (black: 3 min, purple: 5 min, red: 8 min).

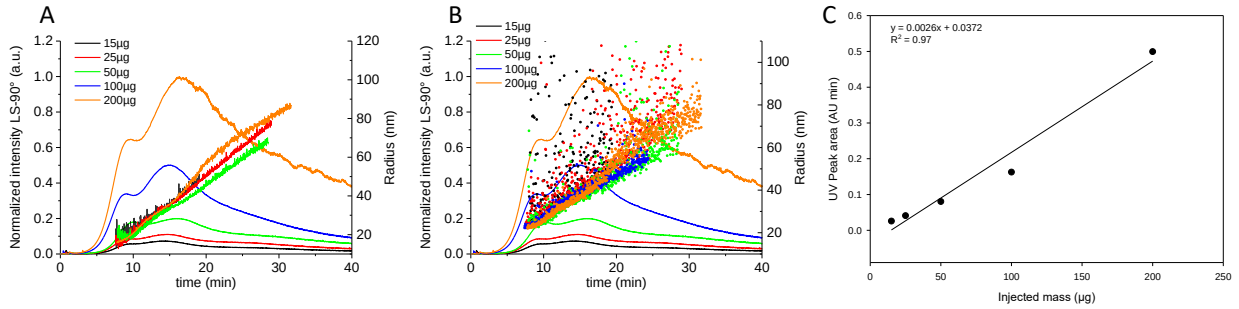

Figure S5: Effect of injected mass for Dox2. Injection of (5 to 200) µg applying the optimized method. A) AF4 fractograms showing normalized excess Rayleigh ratio at 90° versus elution time

with R_g overlaid, B) fractograms with R_h (dots) measured by online QELS overlaid, and C) UV-Vis response reporting the area under the eluted peaks as a function of injected mass.

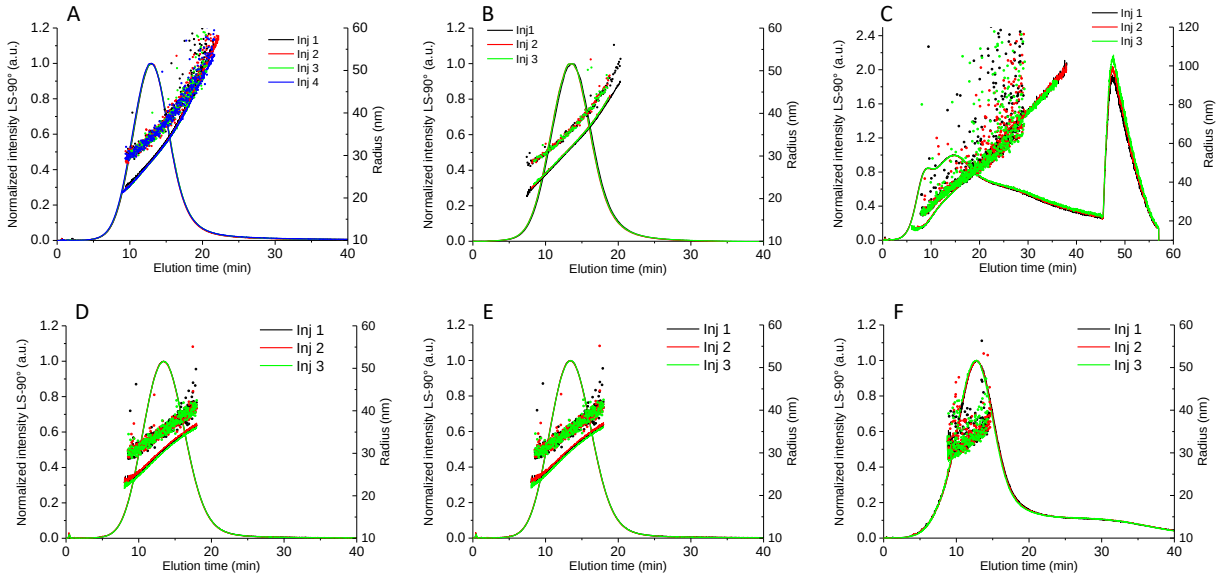

Figure S6: *Repeatability of the optimized method by injecting 3 or more replicate samples. A) Dox1, B) Dox1C, C) Dox2, D) Dox3 E) Dox 4, and F) Cipro. AF4 fractograms showing normalized excess Rayleigh ratio at 90° versus elution time with R_g (line) and R_h (dots) overlaid.*

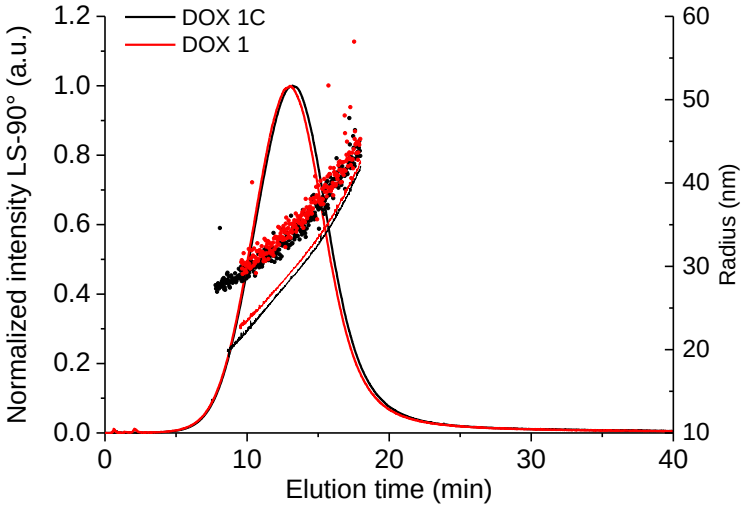

Figure S7: *Comparison of AF4 fractograms showing normalized excess Rayleigh ratio at 90° versus elution time with R_g (lines) and R_h (dots) overlaid, for Dox1 (red) and its control Dox1C (black) using the optimized method.*

6. Supplementary tabular data

Table S1: Composition and pH of mobile phases used in this study. Concentration is reported in g/L. Hydrates are converted to equivalent anhydrous content.

Buffer code	Buffer description	Product number	NaCl	KCl	Na_2HPO4	KH_2PO4	pH[2]	Experiments performed/Lab
PBS1	PBS from Lonza	17-516Q	9	0	0.421	0.144	7.4 ± 0.1	Lab 1: method optimization
PBS2	DPBS from Lonza	17-512F	8	0.2	1.144	0.2	7.3 ± 0.1	Lab 1: method optimization Lab 2: method optimization and analysis of Dox1 with the optimized method
PBS3	PBS from GE Hyclone Classic	16777-252	8	0.2	1.15	0.2	7.2 ± 0.1	Lab 1: method optimization and analysis of the different formulations with the optimized method
PBS4	PBS (tablets) from Gibco, ThermoFisher	10010031	8.12	0.201	0.95	-	7.4 ± 0.1	Lab 3: analysis of Dox1 using the optimized method
Saline	NaCl 0.9% VWR Chemicals BDH	BDH7257-1	9	0	0	-	6.0 ± 0.1	Lab 1: method optimization

[2] pH was measured using InLab Semi-Micro Combination pH electrode and model Mettler Toledo pH meter after calibration with NIST Traceable buffers at ambient temperature.

Table S2: Description of liposomal formulations used in this study as provided by the vendor. Z-avg is the intensity weighted hydrodynamic diameter calculated using cumulants analysis of DLS data. PI is the polydispersity index obtained from cumulants analysis.

Sample code	Sample description	Size (r.nm) and PI	Total API	Total lipid content (mg/mL)	Provider
Dox1	Research grade commercial liposomal doxorubicin hydrochloride product with same P-C properties as RLD Doxil in isotonic sucrose with histidine buffer.	Z-avg= 78 nm PI= 0.06	Doxorubicin HCl at 2.0 mg/mL	15.8	Lipocure LtD batch #101071
Dox1C	Research grade empty control liposomes. In isotonic sucrose with histidine buffer.	Z-avg=78 nm PI= 0.04	0	15.6	Lipocure LtD batch #500010
Dox2	Research grade liposomal doxorubicin hydrochloride. Polymodal and polydisperse product. Contains 10 % sucrose and histidine buffer. Stored frozen.	Z-avg= 135 nm PI= na	Doxorubicin HCl at 2.2 mg/mL	26.8	Avanti polar Product code 300115, lot #300115-01-010
Dox3	Pharmaceutical grade liposomal doxorubicin hydrochloride (generic Doxil) in sucrose with histidine buffer.	na	Doxorubicin HCl at 2.0 mg/mL (<10% free)	15.9	Dr Reddy Laboratories LTD NDC 43598-283-35
Dox4	Pharmaceutical grade liposomal doxorubicin hydrochloride product (generic Doxil) in sucrose with histidine buffer.	na	Doxorubicin HCl at 2.0 mg/mL (<10% free)	15.9	Sun Pharmaceutical Industries LTD NDC 47335-050-40
Cipro	Research grade liposomal ciprofloxacin.	Z-avg= 80 nm, PI=0.1	Ciprofloxacin at 1 mg/mL (<5% free)	20	ProFoldin Lot PHPC002 CP

na=not available

Table S3: MALS angles and positions for Wyatt DAWN HELEOS II MALS and Postnova 3621 MALS

LS Position	Fixed detector angles	
	Wyatt DAWN HELEOS II MALS	Postnova 3621 MALS
1	22.5	7
2	28	12
3	32	20
4	38	28
5	44	36
6	50	44
7	57	52
8	64	60
9	72	68
10	81	76
11	90	84
12	99	90
13	108	100
14	117	108
15	126	116
16	134	124
17	141	132
18	147	140
19		148
20		156
21		164

Table S4: Summary of results obtained by batch mode (off-line) DLS using cumulants analysis (mean hydrodynamic radius (R_h) and polydispersity index (PI)), and the intensity-weighted mean hydrodynamic radius calculated by non-negative constrained least squares analysis (Peak 1). Mean of 5 measurements reported. SD = standard deviation of the mean.

Sample Name	***R*h (SD)**	**PI (SD)**	**Peak 1 (SD)**
	r.nm		r.nm
Dox1	40 (1)	0.06 (0.02)	42.5 (2)
Dox2	56 (2)	0.26 (0.02)	73.5 (9)
Dox3	41 (1)	0.03 (0.02)	43 (1)
Dox4	39 (1)	0.05 (0.01)	41.5 (1)
Cipro	43.5 (1)	0.01 (0.02)	48.5 (4)

Table S5: Summary of results obtained for analysis of Dox1 and applying multiple elution programs at a detector flow DF=0.5 mL/min. Recovery, retention time and retention ratio were measured at an absorbance of 280 nm. R_g was determined using the Berry model with MALS data and R_h were averaged across the FWHM by QELS (Wyatt) at the angle positions 134°. Only one injection for each condition was tested. na=not applicable

Elution programs	DF (mL/min)	Recovery (%)	Retention time (min)	Retention ratio	R_g (nm)	R_g Spread (nm)	R_h (nm)	R_h Spread (nm)	R_g/R_h
Constant XF 0.3	0.5	94	13.5	0.018	29.9	10.3	na	na	na
Constant XF 0.5	0.5	96	24.2	0.010	28.5	14.9	na	na	na
Constant XF1=1 (10 min) XF2=0.5	0.5	96	31.1	0.008	29.3	11.8	na	na	na
Constant XF1=1 (10 min) XF2=0.3	0.5	94	22.3	0.011	29.6	11.2	na	na	na
Exponential 1 => 0 (45min)	0.5	94	19.3	0.013	29.3	11.9	na	na	na
Linear 1 => 0 (45min)	0.5	94	31.3	0.008	30.1	11.0	na	na	na
Linear 0.8 => 0 (45min)	0.5	94	27.4	0.009	29.5	11.8	na	na	na
Linear 1.25 => 0 (45min)	0.5	94	35.5	0.007	30.1	11.4	na	na	na
Linear 1 => 0 (30min)	0.5	98	23.4	0.010	30.9	11.5	34.6	9.7	0.89
Linear XF1 => 0 (60 min)	0.5	95	31.3	0.008	30.2	12.2	35.8	11.2	0.84

Additional measurement conditions: Membrane RC 10 kDa, Long channel, mass injected=50 µg, sample diluted at 1 mg/mL in the elution buffer (DPBS by Lonza), focus flow of 2 mL/min for 8 min.

Table S6: Summary of results obtained for analysis of Dox1 and applying multiple elution programs at a detector flow DF=1 mL/min. Recovery, retention time and retention ratio were measured at an absorbance of 280 nm. R_g was determined using the Berry model. R_g and R_h were averaged across the FWHM by QELS (Wyatt) at the angle positions 134°. Only one injection for each condition was tested.

Elution programs	DF (mL/min)	Recovery (%)	Retention time (min)	Retention ratio	R_g (nm)	R_g Spread (nm)	R_h (nm)	R_h Spread (nm)	R_g/R_h
Constant XF 0.3	1	96	7.3	0.016	30.3	10.5	32.7	7.8	0.93
Constant XF 0.5	1	96	11.8	0.010	30.5	13.7	33.5	10.8	0.91
Constant XF1=1 (10 min) XF2=0.5	1	95	16.5	0.007	30.4	14.6	33.7	10.1	0.90
Linear 1 => 0 (45min)	1	95	18.5	0.006	31.5	14.8	34.4	10.7	0.92
Linear 0.8 => 0 (45min)	1	97	15.6	0.008	31.0	14.4	33.9	10.3	0.91
Linear 1.25 => 0 (45min)	1	97	22.0	0.005	31.6	14.9	33.6	10.6	0.93
Linear 1 => 0 (30min)	1	96	17.5	0.007	30.8	11.7	33.3	7.4	0.92
Linear 1 => 0 (60 min)	1	95	21.4	0.005	30.7	12.4	33.7	7.5	0.91

Additional measurement conditions: Membrane RC 10 kDa. Long channel, mass injected 50 µg, sample diluted at 1 mg/mL in the elution buffer (DPBS from Lonza), focus flow of 2 mL/min for 8 min.

Table S7: Summary of results obtained by injecting Dox1 and applying multiple elution programs at a detector flow rate DF=0.5 or 1 mL/min. Recovery, retention time and retention ratio were measured at an absorbance of 280 nm. The average and spread of R_g (Berry model) and R_h were calculated across the FWHM of the intensity peak by QELS (Wyatt) at the angle positions 134°. The average and standard deviation calculated for 3 replicate injections are reported.

Elution programs	DF (mL/min)	Recovery (%)	Retention time (min)	Retention ratio	R_g (nm)	R_g Spread (nm)	R_h (nm)	R_h Spread (nm)	R_g/R_h
Constant XF 0.3	0.5	95 (1)	13.1 (0.5)	0.019 (0.001)	30.2 (0.1)	11.8 (0.2)	35.9 (0.1)	11.3 (0.4)	0.83 (0.03)
Exponential XF1->0 (60 min)	0.5	93 (0.3)	22.4 (0.1)	0.011 (0.001)	31.2 (0.1)	13.3 (0.1)	36.5 (0.1)	12.2 (0.9)	0.85 (0.03)
Gradient XF1->0 (30 min)	0.5	95 (0.7)	18.1 (0.1)	0.014 (0.001)	29.9 (0.1)	12.1 (0.1)	35.9 (0.3)	11 (1)	0.83 (0.08)
Constant XF 0.3	1	96 (0.1)	7.2 (0.1)	0.016 (0.001)	30.2 (0.1)	10.4 (0.1)	33.2 (0.1)	7.6 (0.6)	0.91 (0.03)
Exponential XF1->0 (60 min)	1	96 (0.1)	13.0 (0.1)	0.009 (0.001)	30.2 (0.4)	13.1 (0.8)	33.6 (0.1)	9.6 (0.5)	0.89 (0.01)
Linear XF1->0 (30 min)	1	97 (0.1)	16.3 (0.1)	0.007 (0.001)	30 (1)	13.3 (0.1)	33.9 (0.1)	9.4 (0.1)	0.89 (0.03)

Additional measurement conditions: Membrane RC 10 kDa. Long channel, mass injected 25 µg, sample diluted at 1 mg/mL in the elution buffer (DPBS from Lonza), focus 2 mL/min for 8 min.

Table S8: Summary of results obtained by injecting the control Dox1C and applying multiple elution programs at a detector flow rate DF=0.5 or 1 mL/min. Recovery, retention time and retention ratio were measured at an absorbance of 280 nm. The average and spread of R_g (Berry model) and R_h were calculated across the FWHM of the intensity peak by QELS (Wyatt) at the angle positions 134°. The average and standard deviation calculated for 3 replicate injections are reported.

Elution programs	DF (mL/min)	Recovery (%)	Retention time (min)	Retention ratio	R_g (nm)	R_g Spread (nm)	R_h (nm)	R_h Spread (nm)	R_g/R_h
Constant XF 0.3	0.5	92 (0.4)	13.2 (0.02)	0.019 (0.001)	32.1 (0.1)	11.9 (0.07)	36.4 (0.1)	10.8 (0.1)	0.88 (0.01)
Exponential XF1->0 (60 min)	0.5	92 (0.8)	18.4 (0.05)	0.014 (0.001)	32.5 (0.1)	12.5 (0.1)	36.4 (0.1)	11.4 (0.2)	0.89 (0.02)
Linear XF1->0 (30 min)	0.5	90 (0.5)	22.9 (0.1)	0.011 (0.001)	32.2 (0.4)	13.2 (0.02)	37.0 (0.1)	12.3 (0.2)	0.87 (0.01)
Constant XF 0.3	1	96 (0.1)	7.5 (0.05)	0.016 (0.001)	32.2 (0.5)	10 (1)	33.4 (0.2)	8 (1)	0.96 (0.01)
Exponential XF1->0 (60 min)	1	97 (0.1)	13.4 (0.1)	0.0089 (0.007)	32.3 (0.2)	12.9 (0.1)	33.3 (0.7)	9.7 (0.7)	0.97 (0.02)
Linear XF1->0 (30 min)	1	94 (0.1)	16.7 (0.04)	0.007 (0.002)	31.8 (0.1)	13.2 (0.07)	33.8 (0.4)	8.4 (0.9)	0.94 (0.01)

Additional measurement conditions: Membrane RC 10 kDa. Long channel, mass injected 25 µg, sample diluted at 1 mg/mL in the elution buffer (DPBS from Lonza), focus 2 mL/min for 8 min.

Table S9: Summary of results obtained measuring the size of NIST Traceable PSL spheres in the range (15-175) nm (nominal radius) and Dox1 using multiple online sizing detectors: Wyatt MALS and online QELS (mounted in position LS-12 (99.9º) or LS-16 (134º)) and Malvern Zetasizer (173º) operated in flow-mode as the final detector. R_s obtained by MALS using the sphere form factor for PSL and R_g determined using the Berry form of the Debye model for Dox1. The hydrodynamic radius (from QELS or Z-Avg/2 from the Zetasizer) are compared to the stated size values at two different detector flow rates (DF=0.5 and DF=1). Mean (standard deviation) are calculated across the FWHM of the fractograms peak.

		DF 0.5			**DF 1**			
Sample	QELS angle	MALS	QELS	Zetasizer	MALS	QELS	Zetasizer	Stated radius
r.nm.		**R_s or R_g (nm)**	**R_h (nm)**	***z-avg*/2 (nm)**	**R_s or R_g (nm)**	**R_h (nm)**	***z-avg*/2 (nm)**	***R* (nm)**
PSL 15	99.9º	14 (1)	15 (1)	17.5 (2)	16 (1)	14.5 (1)	17 (1.5)	15.5 ± 3
	134º	-	-	-	-	-	-	-
PSL 30	99.9º	29.5 (1)	26.5 (1)	29 (1.5)	30 (1)	24 (1)	30.5 (1)	30.5 ± 4
	134º	-	30.5 (1)	-	-	32 (2)	-	-
PSL 62.5	99.9º	62.5 (1)	-	-	62 (1)	-	-	62.5 ± 3
	134º	-	61 (2)	-	-	54 (4)	-	-
PSL 75	99.9º	71.5 (0.5)	51.5 (2)	68.5 (3.5)	31 (0.5)	-	67.5 (1)	75 ± 4
	134º	-	-	-		38 (2)	-	-
PSL 100	99.9º	101.1 (0.5)	62.5 (5)	93.5 (3)	100.5 (0.5)	53 (4)	102 (3.5)	102 ± 6
	134º	-	105 (7.5)	-	-	89 (9)	-	-
PSL 175	99.9º	184 (1.5)	-	-	181 (2)	-	-	175 ± 6
	134º	-	166 (30)	-	-	258 (42)	-	-
Dox1	99.9º	29.4	35	41.5	14.3	13.9	46.5	-
	134º	-	36	-	-	16.5	-	-

Table S10: Summary of results obtained for Dox1 in the long channel applying a detector flow DF=0.5 or 1 mL/min. R_h measured by QELS (Wyatt) at the angle positions 134 and 99°. In the table the recovery, retention time and retention ration were measured at an absorbance of 280 nm. The average and spread of R_g (Berry model) and R_h (single exponential fit) calculated across the FWHM of the peak are reported. Only one injection was conducted for each condition, except where specified. *Average (standard deviation) reported for 5 replicate measurements.

Sample	DF (mL/min)	DLS angle	Recovery (%)	Retention time (min)	Retention ratio	R_g (nm)	R_g Spread (nm)	R_h (nm)	R_h Spread (nm)	R_g/R_h
Dox1*	0.5	134º	97	12.0 (0.1)	0.04 (0.03)	28.7 (0.3)	12.1 (0.2)	34.2 (0.5)	10.9 (1.5)	0.84 (0.02)
Dox1*	0.5	99.9º	98 (1)	11.9 (0.3)	0.04 (0.03)	28.9 (0.3)	11.9 (0.6)	34.2 (0.4)	11.0 (1.4)	0.84 (0.02)
Dox1	1	134º	95	7.6	0.02	28.7	10.9	28.9	5.5	0.99
Dox1	1	99.9º	96.2 (0.1)	7.2 (0.1)	0.01678 (0.0005)	30.2 (0.1)	10.4 (0.1)	33.2 (0.1)	7.6 (0.6)	0.91(0.03)

Additional measurement conditions: constant cross flow XF=0.3 mL/min, injected mass 25 µg, long channel equipped with a 10 kDa RC membrane, applying a focus time of 8 min and a focus flow of 2 mL/min, sample diluted to 1 mg/mL in the elution buffer (PBS from Hyclone).

Table S11: Summary of the results obtained for Dox1 and Dox1C in the long and in the short channel. R_h measured by QELS (Wyatt) at the angle position 99°. Recovery, retention time and retention ratio measured at an absorbance of 280 nm. The average and spread of R_g (Berry model) and R_h (single exponential fit) were calculated across the FWHM of the peak. Only one injection was conducted for each condition, except where specified. *Average (SD) measured over 5 measurements.

Sample	Channel	Recovery (%)	Retention time (min)	Retention ratio	R_g (nm)	R_g Spread (nm)	R_h (nm)	R_h Spread (nm)	R_g/R_h
Dox1	SC	98	15.2	0.03	28.7	14.4	34.0	11.2	0.84
Dox1*	LC	98 (1)	11.9 (0.3)	0.04 (0.03)	28.9 (0.3)	11.9 (0.6)	34.2 (0.4)	11.0 (1.4)	0.84 (0.02)
Dox1C	SC	102	15.9	0.02	31.0	14.6	34.5	11.0	0.89
Dox1C	LC	110	12.8	0.03	28.7	13.1	34.0	10.9	0.84

Additional measurement conditions: constant cross flow XF=0.3 at detector flow DF=0.5 mL/min, injected mass 25 µg, channel equipped with a 10 kDa RC membrane, applying a focus time of 8 min, and a focus flow of 2 mL/min, sample diluted to 1 mg/mL in the elution buffer (PBS from Hyclone).

Table S12: Summary of results obtained for Dox1 and Dox2 in short channel equipped with spacers of 250 µm, 350 µm and 490 µm. R_h measured by a QELS (Wyatt) at the angle position 99°. Recovery, retention time and retention ratio were measured at an absorbance of 280 nm. The average and spread of R_g (Berry model) and R_h (single exponential fit) were calculated across the FWHM of the peak. Only one injection for each condition was tested, except where specified. *Average (standard deviation) reported for 5 replicate measurements. In the case of Dox2, which is composed of multiple populations, the size value calculated at the LS 90° peak maximum are also reported.

Sample	Spacer	Recovery (%)	Retention time (min)	Retention ratio	R_g (nm)	R_g Spread (nm)	R_h (nm)	R_h Spread (nm)	R_g/R_h
Dox1	250 µm	110	6.0	0.06	29.5	10.8	31.5	7	0.94
Dox1*	350 µm	98 (1)	11.9 (0.3)	0.04 (0.03)	28.9 (0.3)	11.9 (0.6)	34.2 (0.4)	11.0 (1.4)	0.84 (0.02)
Dox1	490 µm	101	32.7	0.01	29.8	13.2	33.1	8.1	0.900
Dox2	250 µm	65	Peak 1: 4.5 Peak 2: 7.00	Peak 1: 0.075 Peak 2: 0.05	Peak 1[#]: 24.5 Peak 2[#]: 37.3	FWHM: 55.3	Peak 1*: 28.0 Peak 2*: 36.1	FWHM: 44.6	Peak 1[#]: 0.88 Peak 2[#]: 1.03
Dox2*	350 µm	93 (6)	Peak 1: 8.6 (0.2) Peak 2: 15.0 (0.7)	Peak 1: 0.048 (0.008) Peak 2: 0.027 (0.005)	Peak 1: 20 (2) Peak 2: 35.5 (0.2)	FWHM: 61 (1)	Peak 1: 26 (2) Peak 2: 39 (1)	FWHM: 76 (16)	Peak 1: 0.76 (0.03) Peak 2: 0.90 (0.03) FWHM: 0.72 (0.05)
Dox2	490 µm	62	Peak 1: 21.7 Peak 2: 40.7	Peak 1: 0.02 Peak 2: 0.01	Peak 1: 15.7 Peak 2: 36.2	FWHM:40	Peak 1: 24.0 Peak 2: 35.5	FWHM: 42	Peak 1: 0.67 Peak 2: 1.01

Additional measurement conditions: constant cross flow XF=0.3 at detector flow DF=0.5 mL/min, injected mass 25µg, short channel equipped with a 10 kDa RC membrane, applying a focus time of 8 min, and a focus flow of 2 mL/min, sample diluted to 1 mg/mL in the elution buffer (PBS from Hyclone).

Table S13: Test of multiple membranes. Summary of the results obtained by using (i) 10 kDa and 30 kDa membrane of RC and focus time of 8 min or (ii) 10 kDa membrane of RC and PES and focus time of 5 min. R_h measured by QELS (Wyatt) at the angle position 99°. Recovery, retention time and retention ratio were measured at an absorbance of 280 nm. The average and spread of R_g (Berry model) and R_h (single exponential fit) were determined across the FWHM of the peak. Only one injection for each condition was tested.

Sample	Membrane	Recovery (%)	Retention time (min)	Retention ratio	R_g (nm)	R_g Spread (nm)	R_h (nm)	R_h Spread (nm)	R_g/R_h
Dox1	10 kDa RC	98	15.2	0.03	28.7	14.4	34.0	11.2	0.84
Dox1	30 kDa RC	96	10.5	0.03	26.7	13.5	34.0	9.3	0.78
Dox1	10kDa PES*	84	17.6	0.03	27.8	14.2	34.7	12.6	0.80
Dox1C	10 kDa RC	102	15.9	0.02	31.0	14.6	34.5	11.0	0.89
Dox1C	30 kDa RC	99	11.0	0.05	28.3	11.0	34.7	12.9	0.81
Dox1C	10kDa PES*	70	21.6	0.02	28.5	13.9	35.0	11.3	0.81

*measured using the long channel.

Additional measurement conditions: constant cross flow XF=0.3 at detector flow DF=0.5 mL/min, injected mass 25 µg, long channel equipped with a 350 µm spacer, applying a focus time of 8 min, and a focus flow of 2 mL/min, sample diluted to 1 mg/mL in the elution buffer (PBS from Hyclone).

Table S14: Summary of results for Dox1 using different mobile phases (PBS from Lonza and Hyclone, DPBS from Lonza, NaCl 0.9%). R_h measured by QELS (Wyatt) at the angle position 99°. Recovery, retention time and retention ratio were measured at an absorbance of 280 nm. The average and spread of R_g (Berry model) and R_h (single exponential fit) were determined across the FWHM of the peak.

Sample	Elution Buffer	Recovery (%)	Retention time (min)	Retention ratio	R_g (nm)	R_g Spread (nm)	R_h (nm)	R_h Spread (nm)	R_g/R_h
Dox1	PBS Lonza	108 (1)	12.7 (0.01)	0.027	29.7 (0.1)	11.6 (0.1)	32.3 (0.1)	8.3 (0.5)	0.91 (0.01)
Dox1	DBPS Lonza	106 (1)	13.4 (0.1)	0.021	30.0 (0.1)	11.6 (0.1)	32.7 (0.1)	9.3	0.92 (0.01)
Dox1	PBS Hyclone	101	12.9	0.027	28.6	10.7	34.2	7.4	0.83
Dox1	NaCl 0.9%	98	12.3	0.34	29.9	11.3	32.6	7.2	0.91

Additional measurement conditions: constant cross flow XF=0.3 at detector flow DF=0.5 mL/min, injected mass 25 µg, long channel equipped with a 10 kDa RC and a 350 µm spacer, applying a focus time of 8 min, and a focus flow of 2 mL/min, sample diluted at 1 mg/mL in the elution buffer (PBS from Hyclone).

Table S15: Summary of results obtained for Dox1 and its control Dox1C applying a focus time of 3, 5 or 8 min. R_h measured by QELS (Wyatt) at the angle position 99°. Recovery, retention time and retention ratio were measured at an absorbance of 280 nm. The average and spread of R_g (Berry model) and R_h (single exponential fit) were determined across the FWHM of the peak. Only one injection for each condition was tested, except where specified. *Average (standard deviation) are reported for 5 replicate measurements.

Sample	Focus time (min)	Recovery (%)	Retention time (min)	Retention ratio	R_g (nm)	R_g Spread (nm)	R_h (nm)	R_h Spread (nm)	R_g/R_h
Dox1	3	101	12.27	0.039	28.7	12.2	33.5	9.0	0.86
Dox1	5	101	12.24	0.04	26.6	12.9	33.4	8.7	0.79
Dox1	8*	98 (1)	11.9 (0.3)	0.04 (0.03)	28.9 (0.3)	11.9 (0.6)	34.2 (0.4)	11.0 (1.4)	0.84 (0.02)
Dox1C	3	110	12.88	0.035	27.91	13.9	34.3	9.7	0.81
Dox1C	5	110	12.84	0.03	27.89	12.9	34.0	10.4	0.82
Dox1C	8	100	12.76	0.03	28.66	13.11	34.0	10.9	0.84

Additional measurement conditions: constant cross flow XF=0.3 at detector flow DF=0.5 mL/min, injected mass 25 µg, long channel equipped with a 10 kDa RC membrane and a 350 µm spacer, applying a focus flow of 2 mL/min, sample diluted to 1 mg/mL in the elution buffer (PBS from Hyclone).

Table S16: Summary of results for Dox2 and Dox4, applying a focus time of 3, 5 or 8 min. R_h was measured by QELS (Wyatt) at the angle position 99°. Recovery, retention time and retention ratio were measured at an absorbance of 280 nm. The average and spread of R_g (Berry model) and R_h (single exponential fit) were determined across the FWHM of the peak. Only one injection for each condition was tested, except where specified. *In the case of the Dox2, which is composed of multiple populations, the size value calculated at the LS 90° peak maximum are also reported.

Sample	Focus (min)	Replicates	Recovery (%)	Retention time (min)	Retention ratio	R_g (nm)	R_g Spread (nm)	R_h (nm)	R_h Spread (nm)	R_g/R_h
Dox4	3	1	98	11.3	0.030	30.0	10.5	35.1	12.0	0.85
Dox4	5	1	99	11.1	0.032	29.76	10.6	35.4	8.4	0.84
Dox4	8	4	101 (1)	11.1 (0.06)	0.032 (0.001)	30.0 (0.16)	10.9 (0.1)	35.0 (0.2)	10.3 (0.7)	0.85 (0.01)
Dox2	3	3	84 (5)	Peak 1: 8.4 (0.04) Peak 2: 14.5 (0.3)	Peak 1: 0.041 (0.004) Peak 2: 0.023 (0.001)	Peak 1*: 20.0 (0.6) Peak 2*: 35.9 (0.4) FWHM: 45 (2)	FWHM: 60 (4)	Peak 1*: 27 (1) Peak 2*: 38.1 (0.6) FWHM: 61 (6)	FWHM: 76 (8)	Peak 1*: 0.75 (0.04) Peak 2*: 0.94 (0.07) FWHM: 0.74 (0.04)
Dox2	5	3	96 (5)	Peak 1: 9.2 (1.2) Peak 2: 14.5 (0.3)	Peak 1: 0.039 (0.004) Peak 2: 0.025 (0.004)	Peak 1*: 18.8 (0.2) Peak 2*: 35.3 (0.4) FWHM: 49 (1)	FWHM: 66 (3)	Peak 1*: 25.4 (0.3) Peak 2*: 37.7 (0.8) FWHM: 62 (4)	FWHM: 81 (27)	Peak 1*: 0.77 (0.01) Peak 2*: 0.93 (0.02) FWHM: 0.79 (0.03)
Dox2	8	5	93 (6)	Peak 1: 8.6 (0.2) Peak 2: 15.0 (0.7)	Peak 1: 0.048 (0.008) Peak 2: 0.027 (0.005)	Peak 1: 20 (2) Peak 2: 35.5 (0.2) FWHM: 46 (1)	FWHM: 61 (1)	Peak 1: 26 (2) Peak 2: 39 (1) FWHM: 60 (6)	FWHM: 76 (16)	Peak 1: 0.76 (0.03) Peak 2: 0.90 (0.03) FWHM: 0.72 (0.05)

Additional measurement conditions: constant cross flow XF=0.3 at detector flow DF=0.5 mL/min, injected mass 25 µg, long channel equipped with a 10 kDa RC membrane and a 350 µm spacer, applying a focus flow of 2 mL/min, sample diluted to 1 mg/mL in the elution buffer (PBS from Hyclone).

Table S17: Concentration series on Dox1. Summary of results for Dox1 in the (5 to 200) µg range. R_h was measured by QELS (Wyatt) at the angle position 99°. Recovery, retention time and retention ratio were measured at an absorbance of 280 nm. The average and spread of R_g (Berry model) and R_h (single exponential fit) were determined across the FWHM of the peak. Only one injection for each condition was tested, except where specified. *Average (standard deviation) for 5 replicate measurements.

Sample	Mass injected (µg)	Recovery (%)	Retention time (min)	Retention ratio	R_g (nm)	R_g Spread (nm)	R_h (nm)	R_h Spread (nm)	R_g/R_h
Dox1	5	na	13.20	0.04	32.48	6.9	47.1	4.4	0.69
Dox1	15	na	12.30	0.04	22.90	12.0	35.4	9.9	0.64
Dox1	25*	98 (1)	11.9 (0.3)	0.04 (0.03)	28.9 (0.3)	11.9 (0.6)	34.2 (0.4)	11.0 (1.4)	0.84 (0.02)
Dox1	50	na	12.73	0.04	28.56	12.2	33.5	9.3	0.85
Dox1	100	na	12.04	0.03	28.53	12.2	32.4	9.1	0.88
Dox1	200	na	12.69	0.03	29.53	12.6	30.8	8.5	0.95

Additional measurement conditions: constant cross flow XF=0.3 at detector flow DF=0.5 mL/min, long channel equipped with a 10 kDa RC membrane and a 350 µm spacer, applying a focus flow of 2 mL/min for 8 min, sample diluted to 1 mg/mL in the elution buffer (PBS from Hyclone).

Table S18: Summary of results for Dox2 in the (15 to 200) µg injected mass range. R_h was measured by QELS (Wyatt) at position LS-12. Recovery, retention time and retention ratio were measured at an absorbance of 280 nm. The average and spread of R_g (Berry model) and R_h (single exponential fit) were determined across the FWHM of the peak. Only one injection for each condition was tested, except where specified. In the case of Dox2, which is composed of multiple populations, the size value calculated at the LS 90° peak maximum are also reported. *Average (standard deviation) for 5 replicate measurements.

Sample	Mass injected (µg)	Recovery (%)	Retention time (min)	Retention ratio	R_g (nm)	R_g Spread (nm)	R_h (nm)	R_h Spread (nm)	R_g/R_h
Dox2	15	63	Peak 1: 9.1 Peak 2: 13.8	Peak 1: 0.07 Peak 2: 0.04	Peak 1: 21.9 Peak 2: 33.8	FWHM: 28	Peak 1: 26.8 Peak 2: 41.0 FWHM: na	FWHM: 38	Peak 1: 0.81 Peak 2: 0.82
Dox2	25*	93 (6)	Peak 1: 8.6 (0.2) Peak 2: 15.0 (0.7)	Peak 1: 0.048 (0.008) Peak 2: 0.027 (0.005)	Peak 1: 20 (2) Peak 2: 35.5 (0.2)	FWHM: 61 (1)	Peak 1: 26 (2) Peak 2: 39 (1)	FWHM: 56 (16)	Peak 1: 0.76 (0.03) Peak 2: 0.90 (0.03)
Dox2	50	72	Peak 1: 9.4 Peak 2: 15.6	Peak1: 0.04 Peak 2: 0.024	Peak 1: 21.0 Peak 2: 35.3	FWHM: 45	Peak 1: 27.7 Peak 2: 40.0 FWHM: 52	FWHM: 36	Peak 1: 0.76 Peak 2: 0.88
Dox2	100	73	Peak 1: 8.4 Peak 2: 14.3	Peak 1: 0.04 Peak 2: 0.03	Peak 1: 18.0 Peak 2: 37.0	FWHM: 45	Peak 1: 24.0 Peak 2: 40.5	FWHM: 40	Peak 1: 0.77 Peak 2: 0.91
Dox2	200	90	Peak 1: 8.7 Peak 2: 16.3	Peak 1: 0.04 Peak 2: 0.02	Peak 1: 19.7 Peak 2: 40.1	FWHM: 60	Peak 1: 24.2 Peak 2: 40.0	FWHM: 56	Peak 1: 0.81 Peak 2: 1.01

Additional measurement conditions: constant cross flow XF=0.3 at detector flow DF=0.5 mL/min, long channel equipped with a 10 kDa RC membrane and a 350 µm spacer, applying a focus flow of 2 mL/min for 8 min, sample diluted to 1 mg/mL in the elution buffer (PBS from Hyclone).

Table S19: Comparison of results for multiple liposomal formulations using the optimized AF4 method. R_h was measured by QELS (Wyatt) at position LS-12. Recovery, retention time and retention ratio were measured at an absorbance of 280 nm. The average and spread of R_g (Berry model) and R_h (single exponential fit) were determined across the FWHM of the peak. The mean (COV) of at least 3 replicate injections is reported for each parameter.

Sample	Replicates	Recovery (%)	Retention time (min)	R_g (nm)	R_g Spread (nm)	R_h (nm)	R_h Spread (nm)	R_g/R_h
Dox1	5	98 (1)	11.9 (2.5%)	28.9 (1%)	11.9 (5%)	34.2 (1%)	11.0 (12%)	0.84 (2%)
Dox1C	3	92 (0.4)	13.2 (0.2%)	32.1 (0.1%)	11.9 (1%)	36.3 (0.1%)	10.8 (1%)	0.88 (1%)
Dox3	3	102 (3)	12.6 (0.2%)	30.7 (1.3%)	10.0 (1%)	35.5 (0.3%)	10 (10%)	0.86 (1%)
Dox4	4	101 (1)	11.1 (1%)	30.0 (0.5%)	10.9 (1%)	35.0 (0.6%)	10.3 (7%)	0.84 (1%)
Dox2	5	93 (6)	Peak 1: 8.6 (2.3%) Peak 2: 15.0 (5%)	Peak 1: 20 (10%) Peak 2: 35.5 (0.6%) FWHM: 46 (2.2%)	FWHM: 61 (1.6%)	Peak 1: 26 (8%) Peak 2: 39 (2.6%) FWHM: 60 (10%)	FWHM: 76 (21%)	Peak 1: 0.76 (4%) Peak 2: 0.90 (3%) FWHM: 0.72 (7%)
Cipro	3	91 (6)	13.5 (0.4%)	32.7 (1.5%)	10.8 (3%)	35.1 (1%)	8 (12%)	0.932 (0.6%)

*Only for Dox2, the size value calculated at LS 90° peak maxima are also reported.

Table S20: Summary of results obtained for Dox1 and Dox2 (1 mg/mL with or without 10 % FBS), in a long channel (Wyatt) and applying the optimized method. R_h was measured by QELS (Wyatt) at position LS-12. Recovery, retention time and retention ratio were measured at an absorbance of 280 nm. The average and spread of R_g (Berry model) and R_h (single exponential fit) were determined across the FWHM of the peak.

Sample	Replicates	Recovery (%)	Retention time (min)	Retention ratio	R_g (nm)	R_g Spread (nm)	R_h (nm)	R_h Spread (nm)	R_g/R_h
Dox1	5	98 (1)	11.9 (0.3)	0.04 (0.03)	28.9 (0.3)	11.9 (0.6)	34.2 (0.4)	11.0 (1.4)	0.84 (0.02)
Dox1+FBS 10%	1	101	11.02	0.032	29.3	11.7	34.0	9	0.861
Dox2	5	93 (6)	Peak 1: 8.6 (0.2) Peak 2: 15.0 (0.7)	Peak 1: 0.048 (0.008) Peak 2: 0.027 (0.005)	Peak 1: 20 (2) Peak 2: 35.5 (0.2)	FWHM: 61 (1)	Peak 1: 26 (2) Peak 2: 39 (1)	FWHM: 56 (16)	Peak 1: 0.76 (0.03) Peak 2: 0.90 (0.03)
Dox2+ FBS 10%	1	101	Peak 1: 8.85 Peak 2: 14.5	Peak 1: 0.062 Peak 2: 0.038	Peak 1: 18.9 Peak 2: 37.3	FWHM: 55	Peak 1: 29.2 Peak 2: 39.7	FWHM: 70	Peak 1: 0.65 Peak 2: 0.93